Atmospheric
Chemistry
and Physics

Estimation of secondary PM$_{2.5}$ in China and the United States using a multi-tracer approach

Haoran Zhang[1], Nan Li[1], Keqin Tang[1], Hong Liao[1], Chong Shi[2,3], Cheng Huang[4], Hongli Wang[4], Song Guo[5], Min Hu[5], Xinlei Ge[1], Mindong Chen[1], Zhenxin Liu[1], Huan Yu[6], and Jianlin Hu[1]

[1]Jiangsu Key Laboratory of Atmospheric Environment Monitoring and Pollution Control, Jiangsu Collaborative Innovation Center of Atmospheric Environment and Equipment Technology, School of Environmental Science and Engineering, Nanjing University of Information Science & Technology, Nanjing, 210044, China
[2]National Institute for Environmental Studies, Center for Global Environmental Research, Tsukuba, Ibaraki, Japan
[3]Institute of Remote Sensing and Digital Earth, Chinese Academy of Sciences, Beijing, 100094, China
[4]State Environmental Protection Key Laboratory of Formation and Prevention of the Urban Air Pollution Complex, Shanghai Academy of Environmental Sciences, Shanghai, 200233, China
[5]College of Environmental Sciences and Engineering, Peking University, Beijing, 100871, China
[6]Department of Atmospheric Science, School of Environmental Studies, China University of Geosciences, Wuhan, 430074, China

Correspondence: Nan Li (linan@nuist.edu.cn) and Hong Liao (hongliao@nuist.edu.cn)

Abstract. PM$_{2.5}$, generated via both direct emission and secondary formation, can have varying environmental impacts due to different physical and chemical properties of its components. However, traditional methods to quantify different PM$_{2.5}$ components are often based on online or offline observations and numerical models, which are generally high economic cost- or labor-intensive. In this study, we develop a new method, named Multi-Tracer Estimation Algorithm (MTEA), to identify the primary and secondary components from routine observation of PM$_{2.5}$. By comparing with long-term and short-term measurements of aerosol chemical components in China and the United States, it is proven that MTEA can successfully capture the magnitude and variation of the primary PM$_{2.5}$ (PPM) and secondary PM$_{2.5}$ (SPM). Applying MTEA to the China National Air Quality Network, we find that (1) SPM accounted for 63.5 % of the PM$_{2.5}$ in cities in southern China on average during 2014–2018, while the proportion dropped to 57.1 % in the north of China, and at the same time the secondary proportion in regional background regions was ∼ 19 % higher than that in populous regions; (2) the summertime secondary PM$_{2.5}$ proportion presented a slight but consistent increasing trend (from 58.5 % to 59.2 %) in most populous cities, mainly because of the recent increase in O$_3$ pollution in China; (3) the secondary PM$_{2.5}$ proportion in Beijing significantly increased by 34 % during the COVID-19 lockdown, which might be the main reason for the observed unexpected PM pollution in this special period; and finally, (4) SPM and O$_3$ showed similar positive correlations in the Beijing-Tianjin-Hebei (BTH) and Yangtze River Delta (YRD) regions, but the correlations between total PM$_{2.5}$ and O$_3$ in these two regions, as determined from PPM levels, were quite different. In general, MTEA is a promising tool for efficiently estimating PPM and SPM, and has huge potential for future PM mitigation.

1 Introduction

Fine particulate matter (PM$_{2.5}$, with an aerodynamic diameter of less than 2.5 μm) can be categorized into primary and secondary PM$_{2.5}$ according to its formation processes. Primary PM$_{2.5}$ (PPM), including primary organic aerosol (POA), elemental carbon (EC), sea salt and mineral dust, is a direct emission product from the combustion of fossil or biomass fuel, dust blowing and sea spray. Secondary PM$_{2.5}$ (SPM) is mainly generated by the further oxidation of gaseous precursors emitted in anthropogenic and biogenic activities (Zhu et al., 2018; Wang et al., 2019). SPM consists of secondary organic aerosol (SOA) and secondary inorganic aerosol (SIA, including sulfate, nitrate and ammonium). The primary and secondary components of PM$_{2.5}$ have different environmental impacts on air quality, human health and climate change. For example, EC is a typical PPM that can severely reduce atmospheric visibility and greatly influence the weather and climate due to its strong absorption of solar radiation (Bond et al., 2013; IPCC, 2013; Mao et al., 2017). Sulfate, a critical hygroscopic component of secondary PM$_{2.5}$ (SPM), can be rapidly formed in high relative humidity and further leads to grievous air pollution (Cheng et al., 2016; Guo et al., 2014; Quan et al., 2015). Furthermore, sulfate and other hygroscopic PM$_{2.5}$ exert considerable influences on climate change, mostly by changing cloud properties (Leng et al., 2013; von Schneidemesser et al., 2015). In addition, different PM$_{2.5}$ components also have various deleterious impacts on human health due to their toxicities (Hu et al., 2017; Khan et al., 2016; Maji et al., 2018).

To understand the severe PM$_{2.5}$ pollution characteristics in China over the past several years (An et al., 2019; Song et al., 2017; Yang et al., 2016), many observational studies have been conducted on PM$_{2.5}$ components. The basic methods used in such studies are offline laboratory analysis and online instrument measurements, such as those made using an aerosol mass spectrometer (AMS). Observational studies are crucial for exactly identifying aerosol chemical compositions. They represent the most widely used offline approach (Ming et al., 2017; Tang et al., 2017; Tao et al., 2017; Dai et al., 2018; Gao et al., 2018; W. Liu et al., 2018; Wang et al., 2018; Zhang et al., 2018; Xu et al., 2019; Yu et al., 2019), and have been successfully applied to investigate the interannual variations of different aerosol chemical species (Ding et al., 2019; Z. Liu et al., 2018). In terms of online approaches, the AMS is a state-of-the-art method for analyzing different chemical species with high time resolution, and has great application value for diagnosing the causes of haze events in China over the past decade (R. J. Huang et al., 2014; Quan et al., 2015; Guo et al., 2014; Yang et al., 2021; Gao et al., 2021; Hu et al., 2021; Zhang et al., 2022).

Nevertheless, both online and offline measurements require high levels of manpower and are economically costly; for these reasons, these methods are expensive and rarely applied in large-scale regions or for long periods.

A chemical transport model (CTM) is another useful tool to identify the composition characteristics of PM$_{2.5}$. The simulation predicted by a CTM features high spatiotemporal resolution (Geng et al., 2021). Meanwhile, it also provides vertical profiles of diverse chemical species (Ding et al., 2016). However, the results of a CTM are largely dependent on external inputs such as emission inventories, boundary conditions, and initial conditions. The internal parameterizations of itself also significantly influence the final model results (Huang et al., 2021), which leads to uncertainty in the simulated PM$_{2.5}$ and its composition. In addition, the burden of their high computational cost and high storage requirement hinders the universal use of CTMs.

In this study, we develop a novel method, Multi-Tracer Estimation Algorithm (MTEA), with the aim of distinguishing the primary and secondary compositions of PM$_{2.5}$ from routine observation of the PM$_{2.5}$ concentration. Different from traditional CTMs, the MTEA proposed by this study is based on statistical assumption and works in a more convenient way. This algorithm and its application are tested in China and the United States. In Sect. 2, we introduce the structure and principle of MTEA. In Sect. 3, we evaluate the MTEA results, comparing three PM$_{2.5}$ composition datasets: (1) short-term measurements in 16 cities in China from 2012 to 2016, as reported in previous studies; (2) continuous long-term measurements in Beijing and Shanghai from 2014 to 2018; and (3) the IMPROVE network in the United States during 2014 and 2018. Additionally, we compare the MTEA model with one of the most advanced datasets from a CTM in China. Subsequently, in Sect. 4, we investigate the spatiotemporal characteristics of PPM and SPM concentrations in China, explain the unexpected haze events in several cities of China during the COVID-19 lockdown, and discuss the complicated correlation between PM and O$_3$. This study differs from previous works as follows: (1) we develop an efficient approach to explore PPM and SPM with low economic or technique costs and a low computational burden, and (2) we apply this approach to observation data from the MEE (China Ministry of Ecology and Environment) network, offering an unprecedented opportunity to quantify the PM$_{2.5}$ components at large spatial and time scales.

2 Methodology

2.1 Multi-Tracer Estimation Algorithm (MTEA)

In order to distinguish PPM and SPM efficiently from the observed PM$_{2.5}$, we develop a new approach, named Multi-Tracer Estimation Algorithm (MTEA). The multi-tracer (denoted X) is defined as representing multiple primary contributions to PM$_{2.5}$, which mainly results from incomplete combustion of carbonaceous material and flying dust. We select the typical combustion product CO as one tracer to represent the combustion process, and the particles in coarse mode (PM$_{coarse}$, denoted PMC, where PMC $=$ PM$_{10}$ $-$ PM$_{2.5}$) as

the other tracer to track flying dust. Then we combine the CO and PMC to generate the multi-tracer X (Eq. 1), which can represent hybrid primary contributions to PM$_{2.5}$.

$$X = a \times CO + b \times PMC (a + b = 100\%) \quad (1)$$

As shown in Eq. (1), we use a and b to quantify the relative contributions of combustion and dust processes to the PPM. Given that a complicated process such as the combustion of multiple sources is hard to represent via current routine CO observations, we avoid considering the correlation among these sources but focus on the relative weights of the combustion process and flying dust. Meanwhile, the uncertainty resulting from the apportioning coefficients a and b will be further discussed in Sect. 4.5. The values of these coefficients depend on the ratio of the emission intensities of POA + EC (combustion products) and fine-mode dust, as shown below:

$$\frac{a}{b} = \frac{E_{OA} + E_{EC}}{E_{finedust}}$$
$$= \frac{1.2 E_{OC} + E_{EC}}{E_{PM_{2.5}} - (1.2 E_{OC} + E_{EC} + E_{SO_4} + E_{NO_3})}, \quad (2)$$

where E_{OA}, E_{EC}, $E_{finedust}$, E_{OC}, $E_{PM_{2.5}}$, E_{SO_4} and E_{NO_3} represent the emissions of OA, EC, fine-mode dust, OC, PM$_{2.5}$, sulfate and nitrate, respectively. We obtain anthropogenic PM$_{2.5}$, EC and OC emissions in China from the Multi-resolution Emission Inventory for China (MEIC, http://meicmodel.org/, last access: 1 August 2021) developed by Tsinghua University (M. Li et al., 2017b). For the United States, we retrieve the emission data from the global inventory HTAP (https://edgar.jrc.ec.europa.eu/htap_v2/index.php?SECURE=123, last access: 1 August 2021). We further estimate the POA emission by multiplying the POC emission by an empirical factor of 1.2, as recommended in the literature (Seinfeld and Pandis, 2006), and we quantify sulfate and nitrate emissions by multiplying the PM$_{2.5}$ emission by an investigative coefficient of 0.1 (Zhang, 2019). However, this investigative coefficient for quantifying primary sulfate and nitrate emissions may be relatively high compared to empirical coefficients (0.01–0.05) used in previous simulation studies. We evaluated the potential effect of the coefficient by conducting a set of comparative simulations with a coefficient of 0.03 and found that the final estimated SPM was not sensitive to this coefficient (Table S1 in the Supplement). Thus, we concluded that the uncertainty of primary sulfate and nitrate emissions did not significantly influence the final estimation of the MTEA model. Other uncertainties of X that are dependent on emission intensities or tracer concentrations are discussed later, in Sect. 4.5. The aim of including coefficient b is to reflect the activity intensity of fine-mode dust by counting the emissions of this dust. However, the MEIC does not directly provide fine-mode dust emissions. It is included in the emissions of total PM$_{2.5}$ (M. Li et al., 2017a). Thus, we inferred the fine-mode dust emission by deducting the emis-

sions of EC, POA, sulfate and nitrate from the PM$_{2.5}$ emissions. Based on Eq. (2), we establish a dynamic a and b value database that reflects the specific changes in PM$_{2.5}$ sources among years, seasons, hours and regions.

With the help of the multi-tracer X, we can describe secondary PM$_{2.5}$ as follows:

$$SPM = PM_{2.5} - PPM \quad (3)$$
$$= PM_{2.5} - \frac{PPM}{X} \times X. \quad (4)$$

Here, PM$_{2.5}$ is the observed PM$_{2.5}$ concentration, and the multi-tracer X can be calculated from the observed CO, PM$_{2.5}$ and PM$_{10}$ concentrations. The original concentrations of CO, PM$_{2.5}$ and PM$_{10}$ are normalized to avoid any influence of their initial levels. To calculate the SPM, the key step is to find the target ratio of PPM/X. In the MTEA method, we give the PPM/X ratio a reasonable range (0–400 is used in this work) and then scan the ratio with an interval of 1. For more precise results, a smaller scanning step can be applied, although this may lead to a larger calculation cost. As a result, each varying ratio may give a series of SPM, along with a coefficient of determination (R^2) between SPM and X (Fig. S1 in the Supplement). If we assume that the PPM and SPM came from different sources or processes, then the appropriate PPM/X ratio should be the one that corresponds to weak correlation between SPM and the tracer X. To aid understanding of the principle of the MTEA approach, we show a flow chart in Fig. 1. We also provide the MTEA software package and input datasets at http://nuistairquality.com/m_tea (last access: 1 August 2021).

The MTEA approach makes some improvements by using a similar principle and similar assumptions to the modified EC-tracer method developed by Hu et al. (2012). They estimated primary and secondary organic carbon (denoted POC and SOC) concentrations by adopting a POC/EC ratio when SOC was least strongly correlated with EC. However, this assumption may be too hard to achieve in the real atmosphere. Therefore, in the MTEA approach, we take a range of proper ratios of PPM/X when SPM correlates with the tracer X nonsignificantly (with a p-value greater than 0.05). As a result, the calculated SPM concentration for each case is a range (Table S2 in the Supplement). We employ the concentration ranges to represent the severity of secondary pollution and discuss its uncertainties in the following discussions. For quantitative calculations, the mean values of the concentration ranges are used for the final estimation.

2.2 PM$_{2.5}$ measurements

2.2.1 PM$_{2.5}$ concentration measurements from the MEE network in China

Focusing on the PM$_{2.5}$ pollution in China, MEE set up a comprehensive air quality monitoring network that has permitted consistent access to hourly concentrations of PM$_{2.5}$
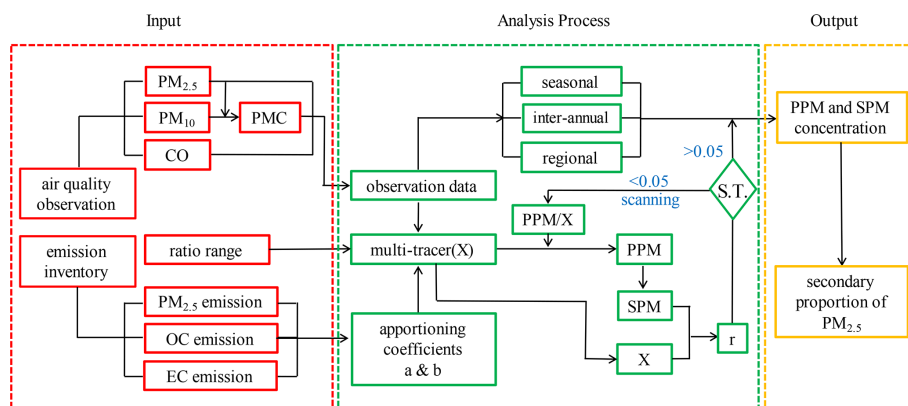
Figure 1. Flow chart of the MTEA approach. The part in red indicates the air quality data and emission input. The part in green represents the key process for predicting PPM and SPM based on routine PM$_{2.5}$ observation; in this part, S.T. refers to the significance test. The significant level α is set to 0.05. The part in orange indicates the final output.

as well as SO$_2$, NO$_2$, CO, O$_3$ and PM$_{10}$ since 2013. This network is currently the most advanced monitoring network in China. In this study, we obtained hourly surface observations of PM$_{2.5}$, PM$_{10}$, CO and O$_3$ at 334 national monitoring sites in 50 cities from 2014 to 2018 from the MEE public website (http://106.37.208.233:20035/, last access: 1 August 2021). Among those 50 cities, 31 are provincial capital cities, which were included to represent populous cities, while the other 19 are relatively small cities that are categorized as regional background cities (Table S3 in the Supplement). Except for Guyuan, the mean PM$_{2.5}$ concentration in each regional background city is less than 35.0 μg m^{-3} (Chinese National Ambient Air Quality Standard level II, NAAQS), indicating that they are only slightly impacted by anthropogenic activities. By comparing the populous cities with the regional background cities, we can reveal the discrepancy in PPM and SPM between regions that suffer from different levels of PM$_{2.5}$ pollution. The geographical distribution of these populous and regional background cities is shown in Fig. 2a.

Recently, the Chinese government carried out a series of control policies, such as the elimination of backward industry, desulfurization and denitration of flue gas, as well as restrictions on motor vehicles (Tang et al., 2019; Wu et al., 2017). Consequently, the concentrations of the major gaseous and particle pollutants have been decreasing year by year (Zhai et al., 2019; Shen et al., 2020). Taking PM$_{2.5}$ as an example, previous studies revealed that the annual mean PM$_{2.5}$ decreased by 30 %–50 % across China during the period of 2013–2018.

2.2.2 PM$_{2.5}$ composition measurements in China

Numerous studies focusing on the aerosol chemical composition in China have employed offline filter-based observations coupled with laboratory analysis to obtain detailed information on PM$_{2.5}$ compositions. To directly compare the estimated with the measured PPM or SPM in China, we per-

formed an evaluation based on two long-term time series of in situ measurements taken in Beijing (Peking University, PKU) and Shanghai (Shanghai Academy of Environmental Sciences, SAES) during 2014–2018 (Huang et al., 2019; Tan et al., 2018). The chemical composition measurements included ions (NH$_4^+$, Na$^+$, K$^+$ Mg^{2+}, Ca^{2+}, SO$_4^{2-}$, NO$_3^-$ and Cl$^-$, measured by ion chromatography), elements (Al, Si, Ti, Ca, Ti, Mn, etc., measured by X-ray fluorescence spectrometry) and carbonaceous components (EC and organic carbon, measured using a thermal-optical transmittance carbon analyzer). After accessing the chemical compositions, we categorized them into PPM and SPM for further evaluation. Specifically, SOA was roughly identified from organic matter (OM) by the EC-tracer model (Ge et al., 2017). SPM concentrations were calculated by summing the SO$_4^{2-}$, NO$_3^-$, NH$_4^+$ and SOA concentrations. Then PPM was calculated by deducting SPM from PM$_{2.5}$.

In addition, we investigated observation-based analyses of PM$_{2.5}$ components in 16 cities in China during 2012–2016 from 32 published studies. This survey offered an opportunity to compare the estimations from MTEA with past measurements of the secondary fraction of PM$_{2.5}$. SOA concentrations in the literature were roughly estimated by multiplying the OM by 0.5 because of limited access to the source data. Meanwhile, it should be noted that the factor that can convert OC (organic carbon) to OM is dependent on the definitions used in a specific observation study.

2.2.3 PM$_{2.5}$ composition measurements from the IMPROVE network in the United States

The Interagency Monitoring of Protected Visual Environments (IMPROVE) aerosol network has continuous records of PM$_{10}$ and PM$_{2.5}$ and PM$_{2.5}$ chemical speciation in the United States since 1987. The specific aerosol chemical compositions include ammonium sulfate, ammonium nitrate, organic carbon, EC, soil dust and mineral dust. The catego-
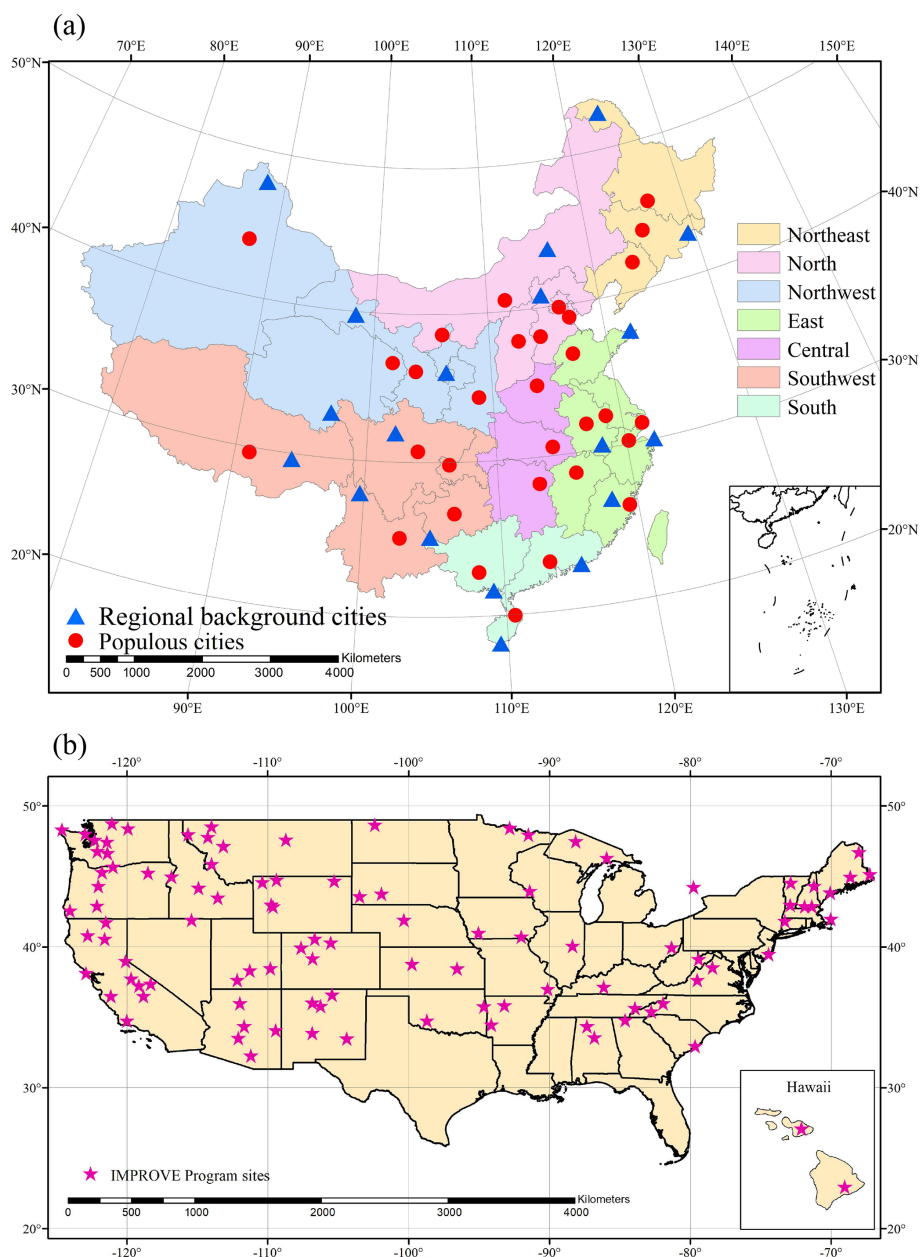
Figure 2. The geographical locations of the observational data used in this study. **(a)** Geographical locations of the 31 populous cities (red circles) and 19 regional background cities (blue triangles) in China considered in this study. **(b)** Spatial distribution of the IMPROVE aerosol monitoring network (pink pentagrams) in the United States.

rization process for PPM and SPM in the IMPROVE dataset is similar to the process described in Sect. 2.2.2. The only difference is that the SPM concentration is the sum of ammonium sulfate, ammonium nitrate and SOA. More detailed descriptions of IMPROVE are available at http://vista.cira. colostate.edu/Improve/ (last access: 1 August 2021). In the present study, we extracted measurements for 104 valid sites in the United States from 2014 to 2018 to evaluate MTEA. The spatial distribution of the IMPROVE sites used in this work is shown in Fig. 2b. It should be noted that the IM-

PROVE program only provides a single aerosol component profile every 3 d. We lowered the time resolution to the monthly average for further evaluation. However, CO is excluded from the IMPROVE program. We therefore adopted the Kriging interpolation of CO data based on the hourly archives from the United States EPA (https://www.epa.gov/outdoor-air-quality-data, last access: 1 August 2021) as an alternative for model input when running MTEA.

2.3 PPM and SPM estimated by a CTM

Apart from evaluating PPM and SPM with various composition measurements, we also compared MTEA estimations with CTM results. Here, we utilized the PM$_{2.5}$ composition gridded dataset with a spatial resolution of $10\,\mathrm{km} \times 10\,\mathrm{km}$ developed by Tsinghua University for further comparisons. This dataset is named Tracking Air Pollution in China (TAP, available at http://tapdata.org.cn/, last access: 15 March 2022) (Geng et al., 2021, 2017). The TAP reanalysis dataset is originally based on CMAQ (Community Multiscale Air Quality) simulation and is further assimilated by ground measurements, satellite remote sensing retrievals and emission inventories with the aid of machine learning algorithm. We collected the monthly mean concentrations of aerosol species during 2014–2018 from TAP, including SO$_4^{2-}$, NO$_3^-$, NH$_4^+$, OM, BC (black carbon) and total PM$_{2.5}$. SOA was further calculated from OM by the EC-tracer model (Ge et al., 2017). SPM concentrations were inferred by summing SO$_4^{2-}$, NO$_3^-$, NH$_4^+$ and SOA. PPM concentrations were then obtained by deducting SPM from PM$_{2.5}$.

3 Model evaluation

3.1 Evaluation in China

3.1.1 Comparison with continuous long-term measurements in Beijing and Shanghai

We compared the MTEA results with the two sets of long-term in situ measurements in Beijing and Shanghai, China, and the evaluations are shown in Fig. 3. Reduced major axis (RMA) regression was applied to fit the data. Given the discrepancy in PM$_{2.5}$ concentrations between the in situ measurements at a single site and multiple MEE national sites, we first preprocessed the data for further evaluation. In data preprocessing, we removed the in situ daily measurements with values that were over $30\,\mu\mathrm{g\,m^{-3}}$ higher than the city average (from MEE).

Comparisons between the estimated and observed PPM in the two cities are given in Fig. 3a and c. The correlation coefficient r for predicted PPM versus observed PPM is 0.85 for Beijing and 0.87 for Shanghai. The slope of the regression is 1.29 for Beijing and 0.73 for Shanghai, which indicates an overestimation (NMB = 32 %) and underestimation (NMB = −9 %) for these two cities, respectively. For SPM, the regression line for Shanghai is quite close to the 1 : 1 ratio line ($s = 1.13$, $d = -2.3$), and its statistical correlation is up to 0.89. The estimated SPM in Beijing also shows a high correlation with the observed SPM, with its r value exceeding 0.80, though the fitting formula indicates an underestimation of 27 %. These discrepancies can be explained by the fact that the observations of primary emission tracers and PM$_{2.5}$ are obtained from different sites. Specifically, the CO and PMC observations are obtained from 12 monitoring MEE sites in Beijing, while the PM$_{2.5}$ component measurements are from
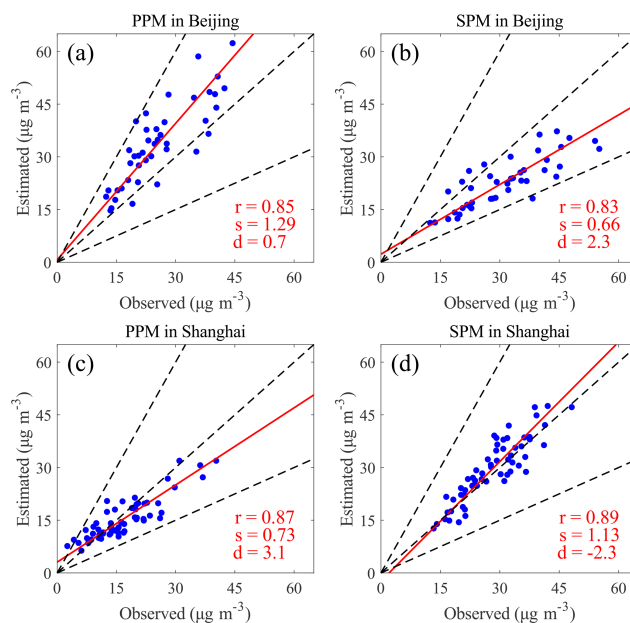
Figure 3. Evaluation of the scatter between the monthly mean of the observed PM and that of the estimated PM in Beijing (**a–b**) and Shanghai (**c–d**), China. Panels (**a**) and (**c**) refer to the PPM, and panels (**b**) and (**d**) refer to the SPM. The red numbers in each panel indicate the Pearson correlation coefficient (r), the slope (s) and the intercept of the fit line (d). The red fit lines are based on reduced major axis (RMA) regression. The dashed black lines in each panel represent, from left to right, the ratios 2 : 1, 1 : 1 and 1 : 2, respectively.

a single spot at PKU that is away from crowded streets (Tan et al., 2018). The MTEA predictions based on the data from MEE sites located in districts with high emission densities may lead to considerable overestimation of PPM concentrations.

Overall, the MTEA model performed satisfactorily in the comparison with long-term in situ measurements in Beijing and Shanghai. Nearly all the points in the plots are located at the range between the ratios 2 : 1 and 1 : 2. It is believed that our model is able to capture the magnitudes and variations of PPM and SPM. The estimated and the observed interannual variations in PPM and SPM are further compared in Sect. 4.2.2.

3.1.2 Comparison with various short-term measurements

To evaluate the reliability of the MTEA approach, we also conducted a literature review in which a variety of observation-based analyses of PM$_{2.5}$ components in 16 cities of China during 2012–2016 were collected (Chen et al., 2016; Du et al., 2017; Cui et al., 2015; Dai et al., 2018; Gao et al., 2018; G. Huang et al., 2014; R. J. Huang et al., 2014; Huang et al., 2017; Jiang et al., 2017; Li et al., 2016; L. Li et al., 2017; Lin et al., 2016; Liu et al., 2017, 2014; W. Liu

et al., 2018; Z. Liu et al., 2018; Ming et al., 2017; Niu et al., 2016; Tan et al., 2016; Tang et al., 2017; Tao et al., 2017, 2015; Tian et al., 2015; Wang et al., 2018; H. L. Wang et al., 2016; Y. Wang et al., 2016; Wu et al., 2016; Xu et al., 2019; Yu et al., 2019; Zhang et al., 2015, 2018; Zhao et al., 2015). Most field measurements focused on regions in eastern China and on episodes during the winter. We list the observed concentrations of PM$_{2.5}$, SO$_4^{2-}$, NO$_3^-$, NH$_4^+$ and SOA from these studies in Table S4 in the Supplement. It should be noted that there may be inconsistencies between the observations due to differences in sampling locations, observation times and analytical instruments between studies.

The estimated PPM and SPM from MTEA show reasonable agreement with the observation-based PM$_{2.5}$ component analyses in China. The MTEA-estimated secondary proportions of PM$_{2.5}$ (i.e., secondary PM$_{2.5}$ / total PM$_{2.5}$) vary in the range of 41 % to 67 % and are higher in eastern cities in China, consistent with the observational results. However, we find that there are still a few discrepancies between the estimated and observation-based results. For example, we overestimated the secondary proportions of PM$_{2.5}$ in cities such as Haikou, Lanzhou and Lhasa. Though all of these show considerable overestimations of over 20 %, the cause of this bias may be quite different for each city. In the coastal city of Haikou, we may attribute this discrepancy between MTEA and observations to the neglect of the contribution of sea salt aerosols. Offline PM$_{2.5}$ measurements in 2015 showed that the contribution of sea salt aerosols to the ambient PM$_{2.5}$ mass concentration in Haikou is 3.6 %–8.3 % (Liu et al., 2017). Secondly, the overestimation phenomenon in Lanzhou, which is a typical inland city located in northwestern China, can be explained by the neglect of the contribution of natural dust to PM$_{2.5}$ speciation. Generally, both sea salt and natural dust are categorized as non-anthropogenic processes, and are not accounted for by the anthropogenic emission inventory, resulting in an underestimation of the primary process intensity. Finally, for Lhasa, the observation-based results are derived from too few samplers, leading to a controversial comparison with the MTEA model.

3.1.3 Comparison with the CTM simulation

In addition to evaluating our model via PPM and SPM measurements in China, we also provide a comparison between MTEA estimation and CTM simulation for 31 populous cities based on monthly mean PM concentrations. As shown in Fig. 4a–b, the correlation coefficient r for TAP versus MTEA is 0.86 in terms of PPM concentration and 0.91 in terms of SPM concentration, showing a strongly positive correlation between the two models. At the same time, both the slopes (1.26 and 0.89) and intercepts (-3.7 and $1.9\,\mu\mathrm{g\,m}^{-3}$) of the regressions about PPM and SPM illustrate that most of the scattered points are distributed around the 1 : 1 ratio line.

Moreover, we further compared MTEA and TAP in terms of the long-term trends in the PPM and SPM concentrations averaged across 31 populous cities (Fig. 4c–d). Both MTEA and TAP exhibit descending interannual trends in the PPM concentration, with rates of -2.0 and $-1.9\,\mu\mathrm{g\,m}^{-3}\,\mathrm{yr}^{-1}$ for MTEA and TAP, respectively. For the SPM concentration, the rates of decline are -2.9 and $-2.8\,\mu\mathrm{g\,m}^{-3}\,\mathrm{yr}^{-1}$, respectively. Meanwhile, the statistical correlations between the two interannual variations are 0.98 (PPM) and 0.99 (SPM), which are both quite close to 1, showing good agreement.

Thus, comparisons of the PPM and SPM concentration magnitudes and interannual variations between the two kinds of models suggest that our statistical model can infer similar estimations to those given by a traditional CTM. Meanwhile, they again highlight that our model is capable of capturing reasonable PPM and SPM concentrations. Furthermore, they also show that MTEA can track primary and secondary components of PM$_{2.5}$ using a proxy at a much lower cost when compared to traditional air quality model simulations.

3.2 Evaluation in the United States

Based on the chemical component measurements of the IMPROVE network, we evaluated the performance of the MTEA model for the United States. Figure 5 presents scatter plots of the evaluation results, with the x axis indicating the observed concentrations and the y axis indicating the estimated concentrations. Temporal, spatial and spatiotemporal validations were performed. Each dot represents a monthly mean observed or estimated PM concentration.

Almost all of the dots are located in the region between the 2 : 1 and 1 : 2 dashed lines, indicating that our model is capable of predicting the magnitudes of PPM and SPM in the United States. Based on correlation analysis, we find that the correlation coefficient r for PPM ranges from 0.69 (spatiotemporal validation) to 0.75 (temporal validation), while r reaches up to 0.98 (temporal validation) for SPM. The results reveal that the MTEA approach successfully captured the spatial and temporal variations of PPM and SPM in the United States.

The majority of the dots are distributed around the 1 : 1 dashed line. Based on the fitting results, the slopes for the regression lines vary from 1.12 (spatial validation) to 1.15 (temporal validation) for PPM and from 0.92 (temporal validation) to 0.93 (spatiotemporal validation) for SPM. In general, PPM and SPM show slight overestimation and underestimation, respectively. These discrepancies may result from the influences of the emission inventory. It is reported that emissions of PMC and CO in the United States continuously declined over the past decade (https://www.statista.com/statistics/501298/volume-of-particulate-matter-2-5-emissions-us/, last access: 2 October 2021). Thus, the coefficients a and b derived from the HTAP global emission inventory in 2010 overestimate the contribution of primary emissions during the study period. However, these emissions inevitably have an impact, and we will discuss the uncertainty of the emission inventory
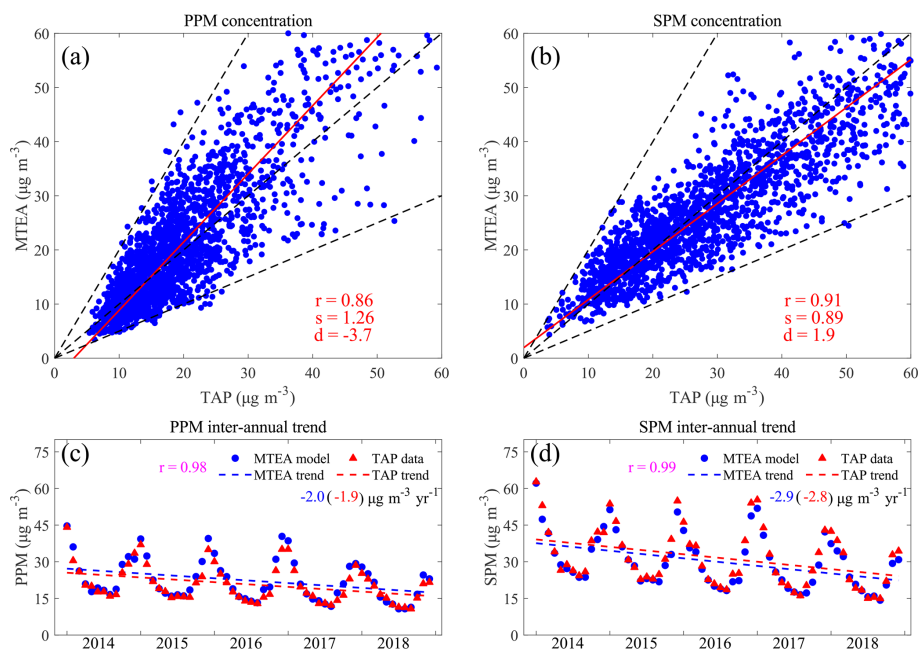
Figure 4. Comparisons between MTEA and TAP in terms of PPM and SPM concentrations and their annual trends from 2014 to 2018 in 31 populous cities in China. In panels **(a)** and **(b)**, each solid blue dot stands for a monthly mean concentration of PPM or SPM in one of the 31 populous cities. The number of samples is 1860 (60 × 31). The metrics r, s and d represent the correlation coefficient, slope and intercept of the fit line, respectively. The fitting method used was reduced major axis (RMA) regression. In panels **(c)** and **(d)**, MTEA and TAP are denoted by blue circles and red triangles, respectively. Each dot represents the mean PPM and SPM concentration across the 31 populous cities. The colored numbers show the annual trends in the PPM and SPM concentrations during 2014–2018. The correlation coefficient (r) of MTEA versus TAP is also provided.
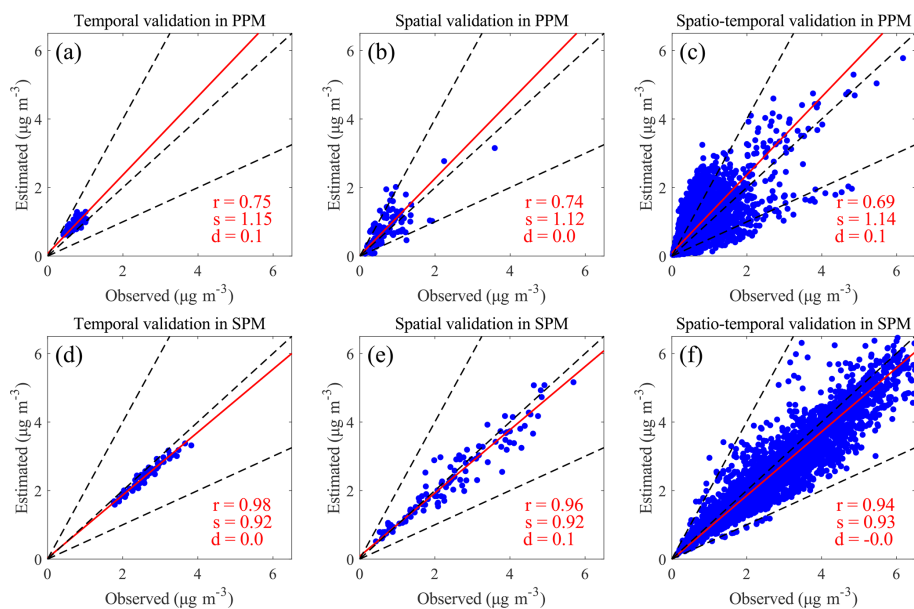
Figure 5. Evaluation of the scatter between the monthly mean of the observed PPM **(a–c)** or SPM **(d–f)** and that of the estimated PPM and SPM in the United States. Panels **(a)** and **(d)**, **(b)** and **(e)**, and **(c)** and **(f)** show temporal, spatial, and spatiotemporal mixed validations, respectively. The red numbers in each panel indicate the Pearson correlation coefficient (r), the slope (s) and the intercept of the fit line (d). The red fit lines are based on RMA regression. The dashed black lines in each panel represent, from left to right, 2 : 1, 1 : 1 and 1 : 2 ratios, respectively.

in Sect. 4.5. In addition, the intercepts of the regression lines for both PPM and SPM are less than $\pm 0.1\,\mu g\,m^{-3}$. The verification results strongly show that our model can reasonably reproduce the monthly averaged concentrations of PPM and SPM in the United States.

4 Results and discussion

We used the MTEA approach and the MEE observation data to estimate PPM and SPM concentrations in China for the period of 2014–2018. Observations during severe haze events (the top 10 % of days for CO and PMC pollution) were excluded to avoid the influence of unfavorable meteorological conditions and extremely high primary emission cases. Unfavorable meteorological conditions are major causes of haze events. Under these unfavored meteorological conditions, PPM may have a considerably collinear relationship with total PM$_{2.5}$. The concentration of SPM from complicated formation pathways is then underestimated. Therefore, we excluded these polluted days to focus more attention on the general characteristics of the PPM and SPM concentrations.

4.1 Spatial distribution

Figure 6 shows spatial patterns of the MTEA-estimated PPM and SPM concentrations over China averaged for the period of 2014–2018. Sixteen populous cities and nine regional background cities in the north, and 15 populous cities and 10 regional background cities in the south (the north and south are separated by the Qinling–Huaihe line) are involved in the following discussions.

In populous cities, the concentrations of both PPM and SPM in the north (the 5-year average is 21.5 for PPM and 26.6 $\mu g\,m^{-3}$ for SPM) are 15 %–43 % higher than those in the south (the 5-year average is 15.0 for PPM and 23.2 $\mu g\,m^{-3}$ for SPM). The north–south difference is mainly caused by the higher energy consumption and consequent stronger pollutant emission in northern populous regions. Nevertheless, in background regions, the difference is relatively small for SPM. The SPM in the south (12.5 $\mu g\,m^{-3}$) is only 1 % higher than that in the north (12.4 $\mu g\,m^{-3}$).

In terms of the secondary proportion of PM$_{2.5}$, the MTEA approach speculates that it is higher in southern regions (63.5 %) than in northern regions (57.1 %). This result confirms the fact that the atmospheric conditions in the south are more favorable for secondary pollutant formation than those in the north. In addition, the MTEA approach captures the difference in the secondary proportion of PM$_{2.5}$ between populous and regional background cities reasonably well. As shown in Fig. 6e and f, the secondary proportion of PM$_{2.5}$ in regional background cities is 19 % higher than that in populous cities, consistent with recent observational studies (Z. Liu et al., 2018). Secondary aerosols can affect a larger area than primary aerosols, mostly due to the diffusion

of their gaseous precursors. Thus, for regional background cities, the role of secondary PM$_{2.5}$ tends to be more important, mainly due to the secondary pollutants transmitted from surrounding populous regions.

4.2 Temporal variation

4.2.1 Seasonal variation

We compare seasonal mean concentrations of the MTEA-estimated PPM and SPM in 31 populous cities and 19 regional background cities in Table 1. The concentrations of both PPM and SPM are the highest in winter, with a seasonal mean concentration of 16.6 for PPM and 24.9 $\mu g\,m^{-3}$ for SPM across China. This phenomenon can be mainly explained by adverse diffusion conditions, such as a low boundary layer height and strong temperature inversion (Zhao et al., 2013), as well as fossil-fuel and biofuel usage for winter home heating (Zhang et al., 2009; Zhang and Cao, 2015). Summer is the least polluted season of the year, with a seasonal mean PPM of 10.2 $\mu g\,m^{-3}$ and SPM of 15.8 $\mu g\,m^{-3}$ nationwide, largely due to the benefits of a higher boundary layer (Guo et al., 2019) and abundant precipitation.

We also compared the secondary proportions of PM$_{2.5}$ in different seasons and in the 50 Chinese cities considered in this work (Table 1). The MTEA approach estimates that the secondary proportion tends to be lowest in fall, with a seasonal mean value of 56.1 % nationwide, while the seasonal proportions stay at around 61 % for the other three seasons. At the same time, the seasonality of the secondary proportion varies among regions. In the north of China, the secondary proportions are higher in spring and summer, which is attributed to the stronger atmospheric oxidizing capacity (AOC) in the warmer seasons. But, in the south of China, the highest secondary proportions occur in winter, which is mainly explained by the tremendous amounts of pollutants (secondary particles and their gaseous precursors) transported from northern China in the presence of the monsoon.

4.2.2 Interannual variation

Figure 7 illustrates the interannual variations of the estimated PPM and SPM based on MTEA in the 31 populous cities and 19 regional background cities of China. We analyzed the MEE observational data during 2014–2018 but excluded the data for 2014 in the regional background regions due to data deficiencies for several cities.

The observed PM$_{2.5}$ concentrations in populous cities have continuously and significantly reduced since 2014, largely due to a series of emission control measures led by the governments, such as the Action Plan on Prevention and Control of Air Pollution (Chinese State Council, 2013). Using the MTEA approach, we find that both PPM and SPM decreased simultaneously at annual rates of decrease of 1.9 and 2.7 $\mu g\,m^{-3}\,yr^{-1}$, respectively. Consequently, the

Table 1. Seasonal mean concentrations of primary and secondary PM$_{2.5}$ in 31 populous cities and 19 regional background cities in China.

City	PPM (µg m^{-3})				SPM (µg m^{-3})				SPM/PM$_{2.5}$ (%)			
	M A M	J J A	S O N	D J F	M A M	J J A	S O N	D J F	M A M	J J A	S O N	D J F
Populous cities in northern China												
Beijing	31.0	28.4	30.6	34.1	25.0	23.7	20.1	16.2	44.7	45.4	39.6	32.2
Tianjin	17.8	13.7	21.9	28.2	42.0	35.3	32.9	29.0	70.2	72.1	60.0	50.7
Shijiazhuang	35.0	22.4	41.5	54.0	36.7	35.5	32.1	37.7	51.2	61.3	43.6	41.1
Taiyuan	22.0	20.2	32.7	32.3	28.4	22.2	21.0	25.0	56.3	52.3	39.1	43.6
Hohhot	13.1	11.4	18.2	20.1	19.2	13.1	16.0	20.7	59.5	53.6	46.8	50.7
Shenyang	21.0	16.7	24.4	27.8	26.1	17.4	20.8	28.0	55.3	51.0	46.0	50.2
Changchun	21.3	15.8	20.2	28.9	18.3	12.3	17.2	25.0	46.2	43.9	46.0	46.4
Harbin	14.1	9.3	15.5	27.2	25.5	15.2	20.9	38.9	64.4	61.9	57.3	58.9
Jinan	25.6	23.0	29.9	32.4	38.2	30.7	30.7	38.3	59.9	57.1	50.7	54.2
Zhengzhou	24.8	20.2	28.6	34.1	45.2	28.8	33.9	44.1	64.6	58.7	54.3	56.4
Lhasa	6.6	5.9	8.2	5.8	13.0	9.2	9.3	13.6	66.3	61.2	53.2	70.1
Xian	24.1	15.3	31.3	37.1	31.5	20.1	24.5	41.3	56.7	56.7	44.0	52.7
Lanzhou	14.1	10.1	17.8	21.3	29.3	24.1	24.8	33.2	67.6	70.4	58.2	60.9
Xining	14.8	12.4	18.3	17.9	26.4	19.3	21.0	34.5	64.1	60.8	53.4	65.9
Yinchuan	12.9	8.2	16.1	18.7	22.8	21.8	21.1	27.0	63.8	72.8	56.7	59.1
Urumqi	15.2	9.5	16.5	27.9	30.9	19.1	32.0	63.6	67.1	66.9	66.0	69.5
Average	19.6	15.2	23.2	28.0	28.7	21.7	23.6	32.3	59.4	58.9	50.4	53.5
Regional background cities in northern China												
Weihai	8.1	7.1	8.6	10.7	23.8	18.5	14.9	13.7	74.6	72.2	63.4	56.0
Jiayuguan	7.8	7.0	7.5	7.0	16.6	11.4	14.5	19.2	68.1	61.9	65.9	73.4
Zhangjiakou	10.8	11.0	10.7	10.7	14.2	14.4	12.8	14.4	56.8	56.6	54.5	57.4
Daxinganling	4.3	3.6	4.6	5.7	9.2	7.7	9.3	11.6	68.0	67.9	67.0	66.9
Xilingol	2.3	2.3	2.8	3.1	10.2	9.3	7.7	9.1	81.8	80.1	73.1	74.7
Yanbian	9.9	5.6	9.4	11.7	15.3	9.1	13.5	17.4	60.7	62.1	58.9	59.7
Guyuan	12.3	9.0	11.9	13.1	19.0	13.1	14.7	20.1	60.7	59.2	55.4	60.6
Yushu	4.3	2.1	4.2	3.9	10.0	9.6	7.1	9.9	69.8	82.3	62.7	71.5
Altay	2.0	1.3	1.7	2.7	6.3	6.3	6.0	8.0	76.1	83.5	77.5	74.7
Average	6.9	5.5	6.8	7.6	13.8	11.1	11.2	13.7	66.9	67.0	62.1	64.2
Populous cities in southern China												
Shanghai	12.4	11.1	11.7	15.8	29.5	22.5	20.8	25.4	70.4	67.0	64.1	61.6
Nanjing	19.1	16.0	19.9	24.3	29.2	18.7	19.9	28.5	60.4	53.9	50.1	54.0
Hangzhou	21.1	17.8	21.5	23.6	24.9	14.5	18.9	28.5	54.1	45.0	46.8	54.7
Hefei	16.4	14.6	17.9	23.2	39.8	26.7	30.1	39.8	70.9	64.6	62.7	63.2
Fuzhou	9.0	7.5	7.5	7.6	18.0	12.9	13.7	19.7	66.6	63.3	64.7	72.2
Nanchang	14.8	9.8	13.2	15.8	20.6	13.6	22.3	28.8	58.2	58.1	62.9	64.6
Wuhan	18.5	15.6	18.9	25.3	36.4	19.9	30.0	45.3	66.3	56.1	61.3	64.2
Changsha	17.6	13.2	17.5	21.9	31.5	21.1	31.2	40.0	64.1	61.5	64.1	64.6
Guangzhou	11.6	9.5	12.1	12.7	22.6	16.3	23.4	26.6	66.0	63.3	65.9	67.7
Nanning	11.7	9.7	14.9	13.3	22.0	12.9	19.9	28.7	65.3	57.1	57.1	68.3
Haikou	5.8	4.7	8.1	6.0	11.5	6.9	8.7	15.8	66.3	59.4	51.8	72.6
Chongqing	17.9	14.0	18.6	21.6	24.1	19.4	25.0	38.8	57.5	58.0	57.3	64.2
Chengdu	29.6	20.0	27.1	31.7	23.6	15.0	18.2	39.1	44.3	42.8	40.1	55.2
Guiyang	13.5	10.6	12.2	9.9	21.3	12.2	18.5	29.8	61.2	53.6	60.4	75.0
Kunming	9.3	6.5	6.9	8.1	21.1	13.5	16.1	18.4	69.5	67.6	69.9	69.3
Average	15.2	12.0	15.2	17.4	25.1	16.4	21.1	30.2	62.2	57.7	58.1	63.5

Table 1. Continued.

City	PPM (µg m^{-3})				SPM (µg m^{-3})				SPM/PM$_{2.5}$ (%)			
	M A M	J J A	S O N	D J F	M A M	J J A	S O N	D J F	M A M	J J A	S O N	D J F
Regional background cities in southern China												
Huangshan	5.3	5.1	5.7	6.4	20.7	11.2	16.3	22.7	79.5	68.8	74.2	78.1
Nanping	6.1	5.0	6.4	5.7	15.9	11.4	13.4	17.4	72.2	69.7	67.9	75.4
Zhoushan	9.5	8.0	8.4	11.9	13.7	10.2	10.1	11.5	59.2	56.2	54.5	49.1
Shanwei	7.9	4.8	8.2	5.7	16.6	10.3	17.4	22.7	67.8	68.2	68.1	79.9
Beihai	7.5	4.2	10.6	8.7	16.4	8.2	16.4	25.8	68.7	65.9	60.6	74.7
Qianxinan	3.3	1.7	2.2	2.9	12.5	12.1	12.2	13.8	79.2	87.9	84.8	82.9
Sanya	4.6	4.2	5.5	3.7	9.7	5.6	6.8	11.7	67.8	56.8	55.4	75.8
Aba	2.0	2.1	2.1	2.9	10.5	10.3	10.3	10.8	84.2	83.0	83.2	78.7
Linzhi	2.3	1.5	2.0	2.1	7.5	6.2	5.3	7.6	76.6	80.5	73.0	78.5
Diqing	1.9	1.5	1.7	1.6	10.5	9.4	9.4	10.2	84.7	86.4	84.8	86.2
Average	5.0	3.8	5.3	5.2	13.4	9.5	11.7	15.4	72.7	71.4	69.1	74.9
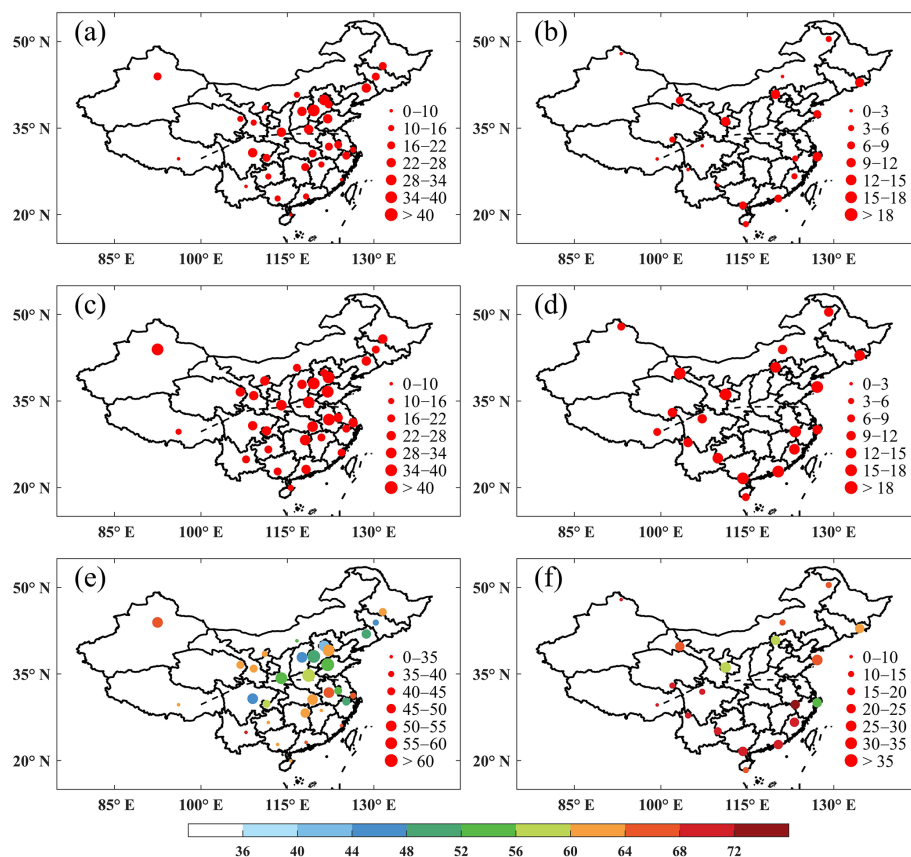
Figure 6. Spatial distributions of PPM (**a, b**), SPM (**c, d**) and the total PM$_{2.5}$ concentration (**e, f**) averaged across the study period. The secondary proportions of PM$_{2.5}$ (SPM / total PM$_{2.5}$) are also shown in (**e**) and (**f**). The left column (**a, c, e**) indicates populous cities. The right column (**b, d, f**) is for the regional background cities. The dotted black line in each panel shows the Qinling–Huaihe line.
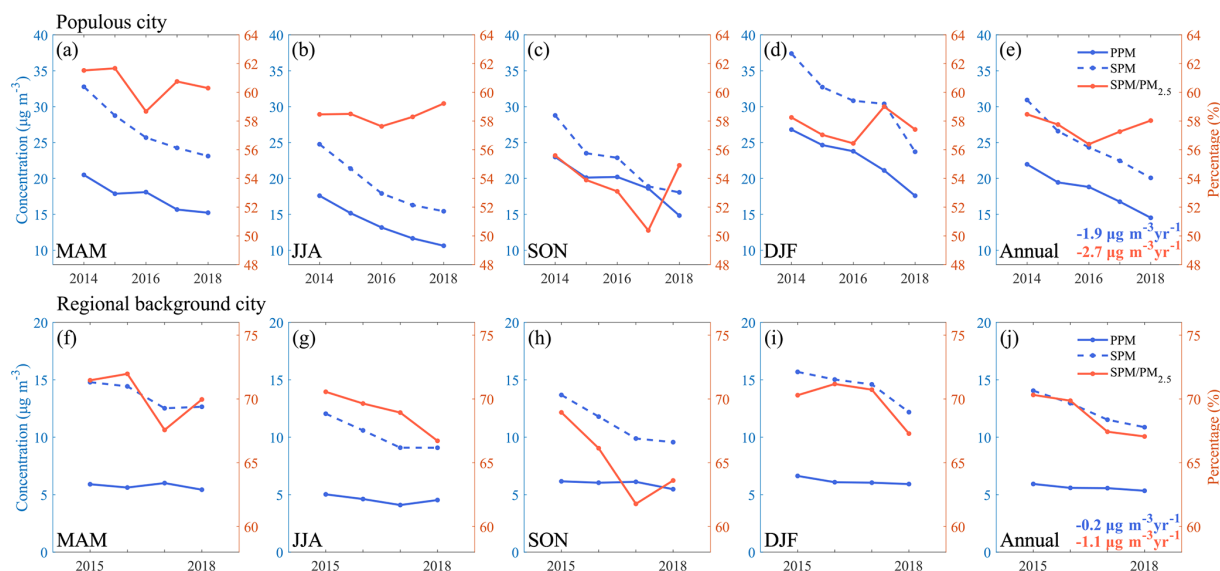
Figure 7. Interannual variations of the PPM concentration (solid blue line), SPM concentration (dotted blue line) and the secondary proportion of PM$_{2.5}$ (solid red line) in populous cities (a–e) and regional background cities (f–j). MAM (a, f), JJA (b, g), SON (c, h) and DJF (d, i) denote spring, summer, fall and winter, respectively. The absolute decreases in PPM and SPM concentration are written in blue and red in panels (e) and (j).

secondary proportion of PM$_{2.5}$ remains relatively constant (56.4 %–58.5 %), but it presents a consistent increasing trend (from 58.5 % to 59.2 %) in summer during the study period, which can be attributed to the continuing worsening O$_3$ pollution (Tang et al., 2022). However, for regional background cities, the MTEA approach reports different features of the PM$_{2.5}$ mitigation. The estimated SPM is considerably reduced by 1.1 µg m^{-3} yr^{-1} in regional background cities, while the PPM remains nearly unchanged (the rate of decrease is 0.2 µg m^{-3} yr^{-1}). This is because the SPM in regional background cities is largely contributed by pollutant transport from surrounding populous regions, where the air quality is getting better as a result of the aforementioned emission controls. However, the PPM mostly derives from local sources and is rarely affected by those emission controls, which mostly focus on densely populated and industrialized cities, not on background regions.

We investigated the interannual variations of PPM and SPM concentrations on the basis of long-term in situ observations in Beijing and Shanghai as well. As Fig. 8 shows, long-term measurements demonstrate a decline in the total PM$_{2.5}$ by 4.0 µg m^{-3} yr^{-1} in Beijing (1.6 for PPM and 2.4 µg m^{-3} yr^{-1} for SPM) and by 3.9 µg m^{-3} yr^{-1} in Shanghai (1.7 for PM and 2.2 µg m^{-3} yr^{-1} for SPM). The observed secondary proportion of PM$_{2.5}$ shows a slight decrease of -0.4 % yr^{-1} in Beijing but a small increase of 0.8 % yr^{-1} in Shanghai. Applying the MTEA model to this case, we are delighted to find that our model not only successfully reproduces the consistent decreasing trends in PPM and SPM in Beijing and Shanghai (the correlation coefficient r of observation versus estimation ranges from 0.83 to 0.89), but

it also captures the different trends in the secondary proportion of PM$_{2.5}$ in the two cities (-0.6 % yr^{-1} in Beijing and 0.3 % yr^{-1} in Shanghai).

4.3 Application during the COVID-19 lockdown

To curb the spread of the novel coronavirus disease 2019 (COVID-19) pandemic, China conducted the first entire city lockdown in Wuhan, Hubei on 23 January 2020. Other provinces also gradually implemented this restriction in the following three weeks (Le et al., 2020). The lockdown greatly limited traffic and outdoor activities, which directly reduced the emissions of primary pollutants (Huang et al., 2020). By analyzing the MEE monitoring data obtained before (1–23 January 2020) and during (24 January to 17 February 2020) the nationwide lockdown (Fig. 9 and Fig. S2 in the Supplement), we show that the national mean NO$_2$, PM$_{2.5}$ and CO concentrations were decreased by 56 %, 30 % and 24 %, respectively, while O$_3$ showed an increase (of 34 %) in general, which would have efficiently promoted the AOC. However, the surface monitoring network still observed unexpected PM$_{2.5}$ pollution in cities over the Beijing-Tianjin-Hebei (BTH) region during the lockdown. Especially in Beijing, the mean PM$_{2.5}$ concentration was increased by $\sim$ 100 % compared to its average value (41 µg m^{-3}) before the nationwide lockdown.

Exploring this unexpected air pollution, we find that the enhanced secondary pollution could be the major factor; this even offset the reduction of primary emissions in the BTH region during the lockdown. With the help of MTEA, we tracked variations of the secondary proportion of PM$_{2.5}$
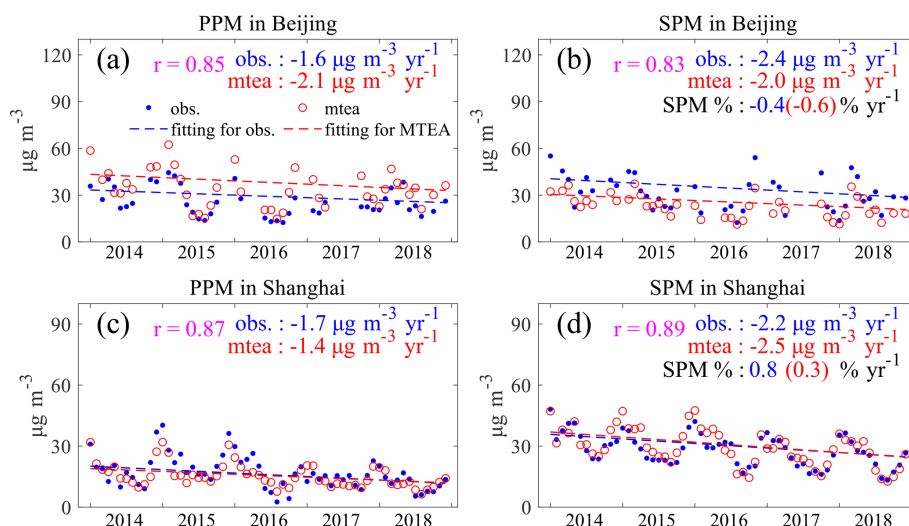
Figure 8. The monthly time series variations of PM in Beijing **(a–b)** and in Shanghai **(c–d)**. Panels **(a)** and **(c)** refer to the PPM and panels **(b)** and **(d)** refer to the SPM. In each panel, in situ observations and MTEA estimations are shown as blue and red dots, respectively. Meanwhile, the dashed blue and red lines show the long-term trends in concentration changes. The rates of decrease in PPM and SPM concentrations as well as the relative changes in the secondary proportions of PM$_{2.5}$ (SPM %) are also provided at the upper right corner of each panel.
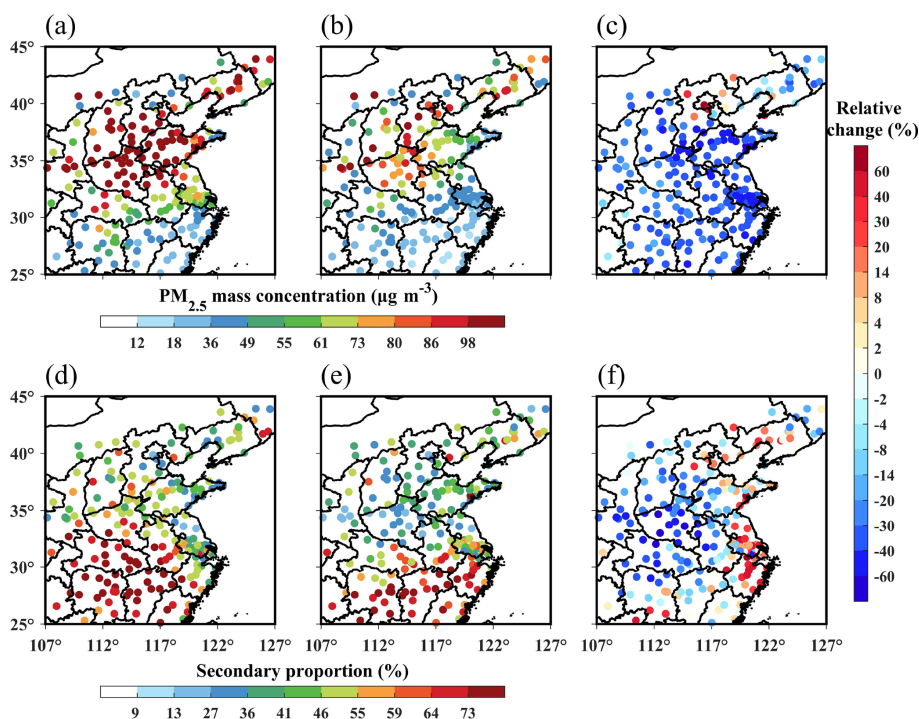
Figure 9. The application of M-TEA to estimate PPM and SPM during the COVID-19 lockdown. Panels **(a)** and **(b)** denote the spatial distribution of the PM$_{2.5}$ mass concentration before the national lockdown (1–23 January 2020, pre-lockdown) and during the national lockdown (23 January to 17 February 2020, post-lockdown). Panel **(c)** indicates the relative change between panels **(a)** and **(b)**, i.e., (post-lockdown − pre-lockdown)/pre-lockdown. Panels **(d)**–**(f)** are the same as panels **(a)**–**(c)** but for the secondary proportions of PM$_{2.5}$.

in East China before and during the COVID-19 lockdown (Fig. 9d–f). The specific emission reductions owing to the national lockdown were derived from Huang et al. (2020). Based on bottom-up dynamic estimation, provincial emissions of CO, NO$_x$, SO$_2$, VOC, PM$_{2.5}$, BC and OC decreased by 13 %–41 %, 29 %–57 %, 15 %–42 %, 28 %–46 %, 9 %–34 %, 13 %–54 % and 3 %–42 %, respectively, during the lockdown period. The secondary proportions in the BTH region show evident increases of 7 %–34 %, which highlight the importance of secondary formation during the lockdown. Our result is consistent with recent observation and simulation studies (Chang et al., 2020; Huang et al., 2020; Le et al., 2020) that suggested that the reduced NO$_2$ resulted in O$_3$ enhancement, further increasing the AOC and facilitating secondary aerosol formation. In addition, another cause of the air pollution was the unfavorable atmospheric diffusion conditions. CO, a nonreactive pollutant, was increased by 22 % in Beijing during the lockdown, even given the considerable reduction in its emission.

For other regions of China, the MTEA approach suggests that the secondary proportion of PM$_{2.5}$ increased by 20 % over the Yangtze River Delta (YRD) region but decreased by 32 % over Central China. Although O$_3$ and AOC enhanced in all these regions, the unprecedented reductions in precursors ultimately resulted in a net drop in secondary pollution.

4.4 Correlation analysis with O$_3$

PM$_{2.5}$ and O$_3$ are closely correlated with each other. One reason for this is that PM$_{2.5}$ and O$_3$ have similar precursors, i.e., NO$_x$ and VOCs. Besides, PM$_{2.5}$ can impact O$_3$ formation by adjusting the radiation balance (Li et al., 2018) and affecting the radical level via aerosol chemistry (Li et al., 2019). There is therefore a complicated interaction between PM$_{2.5}$ and O$_3$. Our study utilized the MTEA approach to explore the relationship between PM and O$_3$ from the perspective of exploring the statistical correlation.

Figure S3 in the Supplement illustrates the hourly correlations between the estimated SPM and the observed O$_3$ averaged for 31 populous cities in China (cities that failed to pass the significance test were excluded) in summer. In general, SPM and O$_3$ show a positive relationship nationwide, especially during the afternoon (during 14:00–18:00, r is up to 0.56). This phenomenon might be explained by noting that the production of O$_3$ and that of SPM are simultaneously affected by AOC; thus, a higher correlation tends to occur when the AOC is stronger. Moreover, the hourly correlations between SPM and O$_3$ are higher than those between PPM and O$_3$ throughout the day, suggesting that secondary oxidation processes may be captured well by the MTEA method.

A series of recent studies have focused on the correlation between PM$_{2.5}$ and O$_3$, and many of them have agreed that the correlation varies greatly among different regions of China. Specifically, the statistical correlation is more positive in southern cities compared to northern cities (Chu et

al., 2020). Because of this significant difference, a question arises: is the difference mostly caused by PPM, by SPM, or by both of them? To address this question, we compared the correlations of daily PPM, SPM and total PM$_{2.5}$ with O$_3$ in the Beijing-Tianjin-Hebei (BTH) and the Yangtze River Delta (YRD) regions during the study period with the help of the MTEA approach. The O$_3$ diurnal formation regime can be destroyed because of the suppressed radiative condition under precipitation. The local O$_3$ concentration level is mainly dominated by background fields. Here, we would like to focus our attention on the secondary formation relationship between daily PM$_{2.5}$ and O$_3$. Therefore, the cases during which precipitation took place were removed to avoid the cleaning impacts of wet deposition on MDA8 (maximum daily 8 h average) O$_3$ concentrations. Precipitation data were based on the ERA5 reanalysis database from the European Centre for Medium-Range Weather Forecasts (ECMWF, https://www.ecmwf.int/, last access: 1 August 2021).

As shown in Fig. 10, the correlations between total PM$_{2.5}$ and O$_3$ are positive and stronger in YRD ($r = 0.14$) than in BTH ($r = 0.09$). However, compared with total PM$_{2.5}$, the correlations between SPM and O$_3$ are much stronger ($r = 0.21$–0.24) and show minor regional differences. The correlation of PPM with O$_3$ is not significant (p-value > 0.05) in either region. The correlation between SPM and O$_3$ is higher mostly because both of them are secondary oxidation products. A higher ambient O$_3$ concentration indicates a stronger AOC, which leads to more SPM generation. However, for PPM, its effect on O$_3$ is mainly to inhibit the production of O$_3$ by adjusting the radiation balance and affecting the radical level. Hence, we suggest that the regional differences in the correlation between total PM$_{2.5}$ and O$_3$ are mainly caused by the different PPM levels in the BTH and YRD regions.

4.5 Uncertainties

Based on the previous evaluation and discussions, we believe that MTEA can successfully capture the magnitudes and spatiotemporal variations of PPM and SPM in China. However, there are still some uncertainties in the model estimation and its application in China.

Firstly, the assumption of nonsignificant correlation between PPM and SPM may be violated by the fact that SO$_2$ and NO$_x$ emitted from combustion will further generate secondary sulfate and nitrate particulates. Nevertheless, the combustion processes for generating SO$_2$ and NO$_x$ and PPM are still different. PPM, i.e., BC and POC, mainly comes from incomplete combustion in residential activities, such as burning biofuels and coal (Long et al., 2013), but SO$_2$ and NO$_x$ mainly come from the complete combustion of industrial and transportation sources, such as coal, gasoline and diesel (Lu et al., 2011; M. Li et al., 2017a; Tang et al., 2019). In addition, the MTEA approach uses the assumption of non-
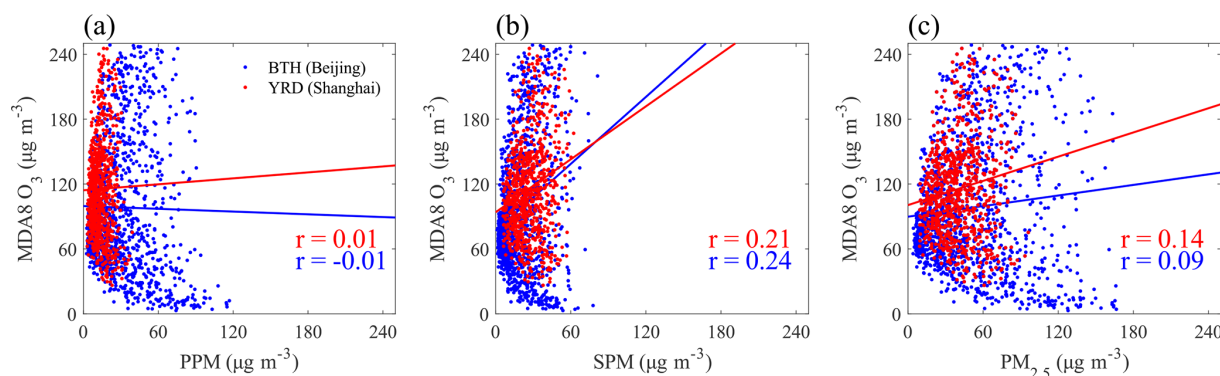
Figure 10. Scatter plots showing the correlation between daily PM concentration and MDA8 O$_3$ concentration in Beijing (blue) and Shanghai (red). Based on the reanalysis dataset ERA5 from ECMWF, days when precipitation took place were removed. Panels **(a)**–**(c)** indicate the PPM, SPM and total PM$_{2.5}$, respectively. In each panel, solid colored lines represent fit lines based on the least squares method. Values of the Pearson correlation coefficient (r) are also given at the bottom right of each panel.

significant correlation rather than irrelevance. Such processing also reduces the uncertainty to a certain extent.

Secondly, natural sources of PPM, such as fine dust from desert and sea salt, are not taken into account in the MTEA approach. As a result, the PPM in a city near a desert or sea could be underestimated. For example, the PM$_{2.5}$ component observational campaign conducted in 2015 showed that the contribution of sea salt aerosols to the ambient PM$_{2.5}$ mass concentration in Haikou is 3.6 %–8.3 % (Liu et al., 2017).

Thirdly, current bottom-up emission inventories are generally outdated, with a time lag of at least 1–2 years, mainly due to a lack of timely and accurate statistics. Consequently, a corresponding uncertainty in MTEA estimation is inevitable. To evaluate the uncertainty, a comparison test was conducted by adjusting the apportioning coefficients (a and b in Eq. 1) with a disturbance of ± 0.1. Firstly, we decreased the value of a in each populous city by 0.1. Meanwhile, the coefficient b was increased by 0.1. This scenario indicates an overestimation of the contribution of combustion-related processes to the primary PM$_{2.5}$ or an underestimation of the contribution of dust-related processes. Secondly, we increased the value of a in each populous city by 0.1 (and decreased b by 0.1) to check the opposite case. The results are presented in Table S5 in the Supplement, and they point out that the estimated secondary proportions of PM$_{2.5}$ varied by less than ± 3 % in the most populous cities due to the changes in the apportioning coefficients. This sensitivity experiment highlights that the apportioning coefficients, which depend on the emissions, have a limited impact on the final estimation results. Generally, the uncertainty of the apportioning coefficients is one of two factors that directly affect the tracer X. The other one is the concentrations of CO and PMC themselves. Hence, we also conducted a similar test to check the impacts of tracer X on the model estimation by changing the tracer concentrations mentioned in Eq. (1). Specifically, we (1) increased the CO concentration by 10 % and decreased the PMC concentration by 10 % and (2) decreased the CO concentration

by 10 % and increased the PMC concentration by 10 %. Both sets of adjustments yield changes of within ± 2 % in the estimated secondary proportions of PM$_{2.5}$ in all cities except for Urumqi (Table S6 in the Supplement). This phenomenon from the perspective of tracer concentration also supports the idea that the impact of the tracer X on the final model results is limited. In summary, we believe that the factor that is most determinative of the final results of our model is the principle of minimum correlation between PPM and SPM, not the tracer X, which relies on emissions or concentrations.

5 Conclusions

In this study, we developed a new approach, MTEA, to distinguish the primary and secondary compositions of PM$_{2.5}$ efficiently from routine observation of the PM$_{2.5}$ concentration with a much lower computation cost than traditional CTMs. By comparing MTEA results with long-term and short-term measurements of aerosol chemical components in China as well as an aerosol composition network in the United States, we showed that MTEA was able to capture variations of PPM and SPM concentrations. Meanwhile, our model showed great agreement with the reanalysis dataset from one of the most advanced CTMs in China as well.

The method was then applied to the surface air pollutant concentrations from the MEE observation network in China, and was found to offer an effective way to understand the characteristics of PPM and SPM across a wide area. In terms of the spatial pattern, MTEA reveals that SPM accounts for 63.5 % of the total PM$_{2.5}$ in southern cities averaged for 2014–2018, while the proportion drops to 57.1 % in the north. It should be noted that the secondary proportion in regional background regions is ~ 19 % higher than that in populous regions. In terms of seasonality, the estimated national averaged secondary proportion is the lowest

in fall (56.1 %), and remains around 61 % during the other three seasons.

Moreover, we applied MTEA to explore the changes in the secondary proportion of PM$_{2.5}$ in China. In recent years, the PM$_{2.5}$ pollution in China has been significantly alleviated, mainly due to a series of emission control measures. The MTEA results suggest that both PPM and SPM decreased simultaneously in populous regions, while for regional background regions, the reduction in secondary PM$_{2.5}$ was much more notable than that in the PPM. The secondary proportion of PM$_{2.5}$ in populous cities during 2014–2018 remained constant (56.4 %–58.5 %) in general on an annual average scale, but it showed a slight but consistent increase in summer, mostly due to the elevated O$_3$ and stronger photochemical pollution in China. In addition, with the help of MTEA, we found that the secondary PM$_{2.5}$ proportion in Beijing significantly increased (by 34 %) during the COVID-19 lockdown, which might be the main reason for the observed unexpected PM pollution in this special period.

Finally, we applied MTEA to explore the synergistic correlation between PM$_{2.5}$ and O$_3$. Estimated results demonstrate that PPM is weakly correlated with O$_3$; its effect on O$_3$ is mainly to inhibit the production of O$_3$ by adjusting the radiation balance and affecting the radical level. SPM is positively correlated with O$_3$ in the presence of the effect of AOC. A higher ambient O$_3$ concentration indicates a stronger AOC, leading to more SPM generation. We suggest that regional differences in the correlation between total PM$_{2.5}$ and O$_3$ are mainly caused by the different PPM levels in the BTH and YRD regions.

We also discussed the uncertainties of the MTEA method. MTEA may overestimate the secondary fractions of PM$_{2.5}$ in regions near to the desert or sea by ~ 20 %, as it fails to take natural dust into consideration. In addition, a sensitivity experiment in which a reasonable disturbance of emissions and tracer concentrations was imposed also showed that such a disturbance has limited impacts on the final estimation. Overall, the factor that is most determinative of our model estimate is the principle of minimum correlation between PPM and SPM.

China has been plagued by PM$_{2.5}$ pollution in recent years. Different PM$_{2.5}$ compositions may have different impacts on the environment, climate and health, due to their different sources and generation pathways. Therefore, it is of great importance to quantify PPM and SPM for pollution recognition and prevention. The methods that are used to quantify different PM$_{2.5}$ components are often based on either lab analysis of offline filter samplings or online observation instruments such as AMS. However, these methods are often labor intensive, highly technical and have a high economic cost. CTM is another useful tool to reveal the composition characteristics of PM$_{2.5}$. However, traditional CTMs also have high hardware requirements. Our study has developed an efficient, lower-cost approach based on a statistical principle to explore PPM and SPM, and applying this approach to large-scale observation networks, such as the MEE network, can offer an unprecedented opportunity to quantify the PM$_{2.5}$ components at large spatial and time scales.

Author contributions. NL designed this study. NL and HL supervised this work. HZ and KT established, performed and improved the MTEA model. HZ and NL interpreted the data and wrote the original draft. CH, HW, SG and MH provided the long-term measurements of aerosol compositions. HL, CS, JH, XG, MC, ZL and HY provided useful comments on the paper, and all authors contributed to the revision of the manuscript.

References

An, Z., Huang, R. J., Zhang, R., Tie, X., Li, G., Cao, J., Zhou, W., Shi, Z., and Ji, Y.: Severe haze in northern China: A synergy of anthropogenic emissions and atmospheric processes, P. Natl. Acad. Sci. USA, 116, 8657–8666, https://doi.org/10.1073/pnas.1900125116, 2019.

Bond, T. C., Doherty, S. J., Fahey, D. W., Forster, P. M., Berntsen, T., DeAngelo, B. J., Flanner, M. G., Ghan, S., Kärcher, B., Koch, D., Kinne, S., Kondo, Y., Quinn, P. K., Sarofim, M. C., Schultz, M. G., Schulz, M., Venkataraman, C., Zhang, H., Zhang, S., Bellouin, N., Guttikunda, S. K., Hopke, P. K., Jacobson, M. Z., Kaiser, J. W., Klimont, Z., Lohmann, U., Schwarz, J. P., Shindell, D., Storelvmo, T., Warren, S. G., and Zender, C. S.: Bounding the role of black carbon in the climate system: A scientific assessment, J. Geophys. Res., 118, 5380–5552, https://doi.org/10.1002/jgrd.50171, 2013.

Chang, Y., Huang, R. J., Ge, X., Huang, X., Hu, J., Duan, Y., Zou, Z., Liu, X., and Lehmann, M. F.: Puzzling Haze Events in China During the Coronavirus (COVID-19) Shutdown, Geophys. Res. Lett., 47, e2020GL088533, https://doi.org/10.1029/2020gl088533, 2020.

Chen, W., Wang, X., Zhou, S., Cohen, J., Zhang, J., Wang, Y., Chang, M., Zeng, Y., Liu, Y., Lin, Z., Liang, G., and Qiu, X.: Chemical Composition of PM$_{2.5}$ and its Impact on Visibility in Guangzhou, Southern China, Aerosol Air Qual. Res., 16, 2349–2361, https://doi.org/10.4209/aaqr.2016.02.0059, 2016.

Cheng, Y., Zheng, G., Wei, C., Mu, Q., Zheng, B., Wang, Z., Gao, M., Zhang, Q., He, K., Carmichael, G., Pöschl, U., and Su, H.: Reactive nitrogen chemistry in aerosol water as a source of sulfate during haze events in China, Sci. Adv., 2, e1601530, https://doi.org/10.1126/sciadv.1601530, 2016.

Chinese State Council: Action Plan on Air Pollution Prevention and Control, http://www.gov.cn/zwgk/2013-09/12/content_2486773.htm (last access: 26 December 2021), 2013 (in Chinese).

Chu, B., Ma, Q., Liu, J., Ma, J., Zhang, P., Chen, T., Feng, Q., Wang, C., Yang, N., Ma, H., Ma, J., Russell, A. G., and He, H.: Air Pollutant Correlations in China: Secondary Air Pollutant Responses to NO$_x$ and SO$_2$ Control, Environ. Sci. Tech. Let., 7, 695–700, https://doi.org/10.1021/acs.estlett.0c00403, 2020.

Cui, H., Chen, W., Dai, W., Liu, H., Wang, X., and He, K.: Source apportionment of PM$_{2.5}$ in Guangzhou combining observation data analysis and chemical transport model simulation, Atmos. Environ., 116, 262–271, https://doi.org/10.1016/j.atmosenv.2015.06.054, 2015.

Dai, Q., Bi, X., Liu, B., Li, L., Ding, J., Song, W., Bi, S., Schulze, B. C., Song, C., Wu, J., Zhang, Y., Feng, Y., and Hopke, P. K.: Chemical nature of PM$_{2.5}$ and PM$_{10}$ in Xi'an, China: Insights into primary emissions and secondary particle formation, Environ. Pollut., 240, 155–166, https://doi.org/10.1016/j.envpol.2018.04.111, 2018.

Ding, A., Huang, X., Nie, W., Chi, X., Xu, Z., Zheng, L., Xu, Z., Xie, Y., Qi, X., Shen, Y., Sun, P., Wang, J., Wang, L., Sun, J., Yang, X.-Q., Qin, W., Zhang, X., Cheng, W., Liu, W., Pan, L., and Fu, C.: Significant reduction of PM$_{2.5}$ in eastern China due to regional-scale emission control: evidence from SORPES in 2011–2018, Atmos. Chem. Phys., 19, 11791–11801, https://doi.org/10.5194/acp-19-11791-2019, 2019.

Ding, A. J., Huang, X., Nie, W., Sun, J. N., Kerminen, V. M., Petäjä, T., Su, H., Cheng, Y. F., Yang, X. Q., Wang, M. H., Chi, X. G., Wang, J. P., Virkkula, A., Guo, W. D., Yuan, J., Wang, S. Y., Zhang, R. J., Wu, Y. F., Song, Y., Zhu, T., Zilitinkevich, S., Kulmala, M., and Fu, C. B.: Enhanced haze pollution by black carbon in megacities in China, Geophys. Res. Lett., 43, 2873–2879, https://doi.org/10.1002/2016gl067745, 2016.

Du, W., Zhang, Y., Chen, Y., Xu, L., Chen, J., Deng, J., Hong, Y., and Xiao, H.: Chemical Characterization and Source Apportionment of PM$_{2.5}$ during Spring and Winter in the Yangtze River Delta, China, Aerosol Air Qual. Res., 17, 2165–2180, 10.4209/aaqr.2017.03.0108, 2017.

Gao, J., Wang, K., Wang, Y., Liu, S., Zhu, C., Hao, J., Liu, H., Hua, S., and Tian, H.: Temporal-spatial characteristics and source apportionment of PM$_{2.5}$ as well as its associated chemical species in the Beijing-Tianjin-Hebei region of China, Environ. Pollut., 233, 714–724, https://doi.org/10.1016/j.envpol.2017.10.123, 2018.

Gao, J., Li, Y., Li, J., Shi, G., Liu, Z., Han, B., Tian, X., Wang, Y., Feng, Y., and Russell, A. G.: Impact of Formation Pathways on Secondary Inorganic Aerosol During Haze Pollution in Beijing: Quantitative Evidence From High-Resolution Observation and Modeling, Geophys. Res. Lett., 48, e2021GL095623, https://doi.org/10.1029/2021gl095623, 2021.

Ge, X., Li, L., Chen, Y., Chen, H., Wu, D., Wang, J., Xie, X., Ge, S., Ye, Z., Xu, J., and Chen, M.: Aerosol characteristics and sources in Yangzhou, China resolved by offline aerosol mass spectrometry and other techniques, Environ. Pollut., 225, 74–85, https://doi.org/10.1016/j.envpol.2017.03.044, 2017.

Geng, G., Zhang, Q., Tong, D., Li, M., Zheng, Y., Wang, S., and He, K.: Chemical composition of ambient PM$_{2.5}$ over China and relationship to precursor emissions during 2005–2012, Atmos. Chem. Phys., 17, 9187–9203, https://doi.org/10.5194/acp-17-9187-2017, 2017.

Geng, G., Xiao, Q., Liu, S., Liu, X., Cheng, J., Zheng, Y., Xue, T., Tong, D., Zheng, B., Peng, Y., Huang, X., He, K., and Zhang, Q.: Tracking Air Pollution in China: Near Real-Time PM$_{2.5}$ Retrievals from Multisource Data Fusion, Environ. Sci. Technol., 55, 12106–12115, https://doi.org/10.1021/acs.est.1c01863, 2021.

Guo, J., Li, Y., Cohen, J. B., Li, J., Chen, D., Xu, H., Liu, L., Yin, J., Hu, K., and Zhai, P.: Shift in the Temporal Trend of Boundary Layer Height in China Using Long-Term (1979–2016) Radiosonde Data, Geophys. Res. Lett., 46, 6080–6089, https://doi.org/10.1029/2019gl082666, 2019.

Guo, S., Hu, M., Zamora, M. L., Peng, J., Shang, D., Zheng, J., Du, Z., Wu, Z., Shao, M., Zeng, L., Molina, M. J., and Zhang, R.: Elucidating severe urban haze formation in China, P. Natl. Acad. Sci. USA, 111, 17373–17378, https://doi.org/10.1073/pnas.1419604111, 2014.

Hu, J., Huang, L., Chen, M., Liao, H., Zhang, H., Wang, S., Zhang, Q., and Ying, Q.: Premature Mortality Attributable to Particulate Matter in China: Source Contributions and Responses to Reductions, Environ. Sci. Technol., 51, 9950–9959, https://doi.org/10.1021/acs.est.7b03193, 2017.

Hu, R., Wang, S., Zheng, H., Zhao, B., Liang, C., Chang, X., Jiang, Y., Yin, R., Jiang, J., and Hao, J.: Variations and Sources of Organic Aerosol in Winter Beijing under Markedly Reduced Anthropogenic Activities During COVID-2019, Environ. Sci. Technol., https://doi.org/10.1021/acs.est.1c05125, 2021.

Hu, W. W., Hu, M., Deng, Z. Q., Xiao, R., Kondo, Y., Takegawa, N., Zhao, Y. J., Guo, S., and Zhang, Y. H.: The characteristics and origins of carbonaceous aerosol at a rural site of PRD in summer of 2006, Atmos. Chem. Phys., 12, 1811–1822, https://doi.org/10.5194/acp-12-1811-2012, 2012.

Huang, G., Cheng, T., Zhang, R., Tao, J., Leng, C., Zhang, Y., Zha, S., Zhang, D., Li, X., and Xu, C.: Optical properties and chemical composition of PM$_{2.5}$ in Shanghai in the spring of 2012, Particuology, 13, 52–59, https://doi.org/10.1016/j.partic.2013.10.005, 2014.

Huang, L., An, J., Koo, B., Yarwood, G., Yan, R., Wang, Y., Huang, C., and Li, L.: Sulfate formation during heavy winter haze events and the potential contribution from heterogeneous SO$_2$ + NO$_2$ reactions in the Yangtze River Delta region, China, Atmos. Chem. Phys., 19, 14311–14328, https://doi.org/10.5194/acp-19-14311-2019, 2019.

Huang, L., Zhu, Y., Zhai, H., Xue, S., Zhu, T., Shao, Y., Liu, Z., Emery, C., Yarwood, G., Wang, Y., Fu, J., Zhang, K., and Li, L.: Recommendations on benchmarks for numerical air quality model applications in China – Part 1: PM$_{2.5}$ and chemical species, Atmos. Chem. Phys., 21, 2725–2743, https://doi.org/10.5194/acp-21-2725-2021, 2021.

Huang, R. J., Zhang, Y., Bozzetti, C., Ho, K. F., Cao, J. J., Han, Y., Daellenbach, K. R., Slowik, J. G., Platt, S. M., Canonaco, F., Zotter, P., Wolf, R., Pieber, S. M., Bruns, E. A., Crippa, M., Ciarelli, G., Piazzalunga, A., Schwikowski, M., Abbaszade, G., Schnelle-Kreis, J., Zimmermann, R., An, Z., Szidat, S., Baltensperger, U., El Haddad, I., and Prevot, A. S.: High secondary aerosol contribution to particulate pollution during haze events in China, Nature, 514, 218–222, https://doi.org/10.1038/nature13774, 2014.

Huang, X., Liu, Z., Liu, J., Hu, B., Wen, T., Tang, G., Zhang, J., Wu, F., Ji, D., Wang, L., and Wang, Y.: Chemical characterization and source identification of PM$_{2.5}$ at multiple sites in the Beijing–Tianjin–Hebei region, China, Atmos. Chem. Phys., 17, 12941–12962, https://doi.org/10.5194/acp-17-12941-2017, 2017.

Huang, X., Ding, A., Gao, J., Zheng, B., Zhou, D., Qi, X., Tang, R., Wang, J., Ren, C., Nie, W., Chi, X., Xu, Z., Chen, L., Li, Y., Che, F., Pang, N., Wang, H., Tong, D., Qin, W., Cheng, W., Liu, W., Fu, Q., Liu, B., Chai, F., Davis, S. J., Zhang, Q., and He, K.: Enhanced secondary pollution offset reduction of primary emissions during COVID-19 lockdown in China, Nat. Sci. Rev., 8, nwaa13, https://doi.org/10.1093/nsr/nwaa137, 2020.

Intergovernmental Panel on Climate Change (IPCC): Climate Change 2013: The Physical Science Basis. Contribution of Working Group I to the Fifth Assessment Report of the Intergovernmental Panel on Climate Change, Cambridge University Press, ISBN 978-92-9169-138-8, 2013.

Jiang, N., Guo, Y., Wang, Q., Kang, P., Zhang, R., and Tang, X.: Chemical Composition Characteristics of PM$_{2.5}$ in Three Cities in Henan, Central China, Aerosol Air Qual. Res., 17, 2367–2380, https://doi.org/10.4209/aaqr.2016.10.0463, 2017.

Khan, M. F., Latif, M. T., Saw, W. H., Amil, N., Nadzir, M. S. M., Sahani, M., Tahir, N. M., and Chung, J. X.: Fine particulate matter in the tropical environment: monsoonal effects, source apportionment, and health risk assessment, Atmos. Chem. Phys., 16, 597–617, https://doi.org/10.5194/acp-16-597-2016, 2016.

Le, T., Wang, Y., Liu, L., Yang, J., Yung, Y. L., Li, G., and Seinfeld, J. H.: Unexpected air pollution with marked emission reductions during the COVID-19 outbreak in China, Science, 369, eabb7431, https://doi.org/10.1126/science.abb7431, 2020.

Leng, C., Cheng, T., Chen, J., Zhang, R., Tao, J., Huang, G., Zha, S., Zhang, M., Fang, W., Li, X., and Li, L.: Measurements of surface cloud condensation nuclei and aerosol ac-

tivity in downtown Shanghai, Atmos. Environ., 69, 354–361, https://doi.org/10.1016/j.atmosenv.2012.12.021, 2013.

Li, H., Wang, Q. g., Yang, M., Li, F., Wang, J., Sun, Y., Wang, C., Wu, H., and Qian, X.: Chemical characterization and source apportionment of PM$_{2.5}$ aerosols in a megacity of Southeast China, Atmos. Res., 181, 288–299, https://doi.org/10.1016/j.atmosres.2016.07.005, 2016.

Li, K., Jacob, D. J., Liao, H., Shen, L., Zhang, Q., and Bates, K. H.: Anthropogenic drivers of 2013-2017 trends in summer surface ozone in China, P. Natl. Acad. Sci. USA, 116, 422–427, https://doi.org/10.1073/pnas.1812168116, 2019.

Li, L., Tan, Q., Zhang, Y., Feng, M., Qu, Y., An, J., and Liu, X.: Characteristics and source apportionment of PM$_{2.5}$ during persistent extreme haze events in Chengdu, southwest China, Environ. Pollut., 230, 718–729, https://doi.org/10.1016/j.envpol.2017.07.029, 2017.

Li, M., Liu, H., Geng, G., Hong, C., Liu, F., Song, Y., Tong, D., Zheng, B., Cui, H., Man, H., Zhang, Q., and He, K.: Anthropogenic emission inventories in China: a review, Natl. Sci. Rev., 4, 834–866, https://doi.org/10.1093/nsr/nwx150, 2017a.

Li, M., Zhang, Q., Kurokawa, J.-I., Woo, J.-H., He, K., Lu, Z., Ohara, T., Song, Y., Streets, D. G., Carmichael, G. R., Cheng, Y., Hong, C., Huo, H., Jiang, X., Kang, S., Liu, F., Su, H., and Zheng, B.: MIX: a mosaic Asian anthropogenic emission inventory under the international collaboration framework of the MICS-Asia and HTAP, Atmos. Chem. Phys., 17, 935–963, https://doi.org/10.5194/acp-17-935-2017, 2017b.

Li, N., He, Q., Greenberg, J., Guenther, A., Li, J., Cao, J., Wang, J., Liao, H., Wang, Q., and Zhang, Q.: Impacts of biogenic and anthropogenic emissions on summertime ozone formation in the Guanzhong Basin, China, Atmos. Chem. Phys., 18, 7489–7507, https://doi.org/10.5194/acp-18-7489-2018, 2018.

Lin, Y. C., Hsu, S. C., Chou, C. C., Zhang, R., Wu, Y., Kao, S. J., Luo, L., Huang, C. H., Lin, S. H., and Huang, Y. T.: Wintertime haze deterioration in Beijing by industrial pollution deduced from trace metal fingerprints and enhanced health risk by heavy metals, Environ. Pollut., 208, 284–293, https://doi.org/10.1016/j.envpol.2015.07.044, 2016.

Liu, B., Li, T., Yang, J., Wu, J., Wang, J., Gao, J., Bi, X., Feng, Y., Zhang, Y., and Yang, H.: Source apportionment and a novel approach of estimating regional contributions to ambient PM$_{2.5}$ in Haikou, China, Environ. Pollut., 223, 334–345, https://doi.org/10.1016/j.envpol.2017.01.030, 2017.

Liu, J., Li, J., Zhang, Y., Liu, D., Ding, P., Shen, C., Shen, K., He, Q., Ding, X., Wang, X., Chen, D., Szidat, S., and Zhang, G.: Source apportionment using radiocarbon and organic tracers for PM$_{2.5}$ carbonaceous aerosols in Guangzhou, South China: contrasting local- and regional-scale haze events, Environ. Sci. Technol., 48, 12002–12011, https://doi.org/10.1021/es503102w, 2014.

Liu, W., Xu, Y., Liu, W., Liu, Q., Yu, S., Liu, Y., Wang, X., and Tao, S.: Oxidative potential of ambient PM$_{2.5}$ in the coastal cities of the Bohai Sea, northern China: Seasonal variation and source apportionment, Environ. Pollut., 236, 514–528, https://doi.org/10.1016/j.envpol.2018.01.116, 2018.

Liu, Z., Gao, W., Yu, Y., Hu, B., Xin, J., Sun, Y., Wang, L., Wang, G., Bi, X., Zhang, G., Xu, H., Cong, Z., He, J., Xu, J., and Wang, Y.: Characteristics of PM$_{2.5}$ mass concentrations and chemical species in urban and background areas of China: emerging results

from the CARE-China network, Atmos. Chem. Phys., 18, 8849–8871, https://doi.org/10.5194/acp-18-8849-2018, 2018.

Long, C. M., Nascarella, M. A., and Valberg, P. A.: Carbon black vs. black carbon and other airborne materials containing elemental carbon: physical and chemical distinctions, Environ. Pollut., 181, 271–286, https://doi.org/10.1016/j.envpol.2013.06.009, 2013.

Lu, Z., Zhang, Q., and Streets, D. G.: Sulfur dioxide and primary carbonaceous aerosol emissions in China and India, 1996–2010, Atmos. Chem. Phys., 11, 9839–9864, https://doi.org/10.5194/acp-11-9839-2011, 2011.

Maji, K. J., Ye, W. F., Arora, M., and Shiva Nagendra, S. M.: PM$_{2.5}$-related health and economic loss assessment for 338 Chinese cities, Environ. Int., 121, 392–403, https://doi.org/10.1016/j.envint.2018.09.024, 2018.

Mao, Y.-H., Liao, H., and Chen, H.-S.: Impacts of East Asian summer and winter monsoons on interannual variations of mass concentrations and direct radiative forcing of black carbon over eastern China, Atmos. Chem. Phys., 17, 4799–4816, https://doi.org/10.5194/acp-17-4799-2017, 2017.

Ming, L., Jin, L., Li, J., Fu, P., Yang, W., Liu, D., Zhang, G., Wang, Z., and Li, X.: PM$_{2.5}$ in the Yangtze River Delta, China: Chemical compositions, seasonal variations, and regional pollution events, Environ. Pollut., 223, 200–212, https://doi.org/10.1016/j.envpol.2017.01.013, 2017.

Niu, X., Cao, J., Shen, Z., Ho, S. S. H., Tie, X., Zhao, S., Xu, H., Zhang, T., and Huang, R.: PM$_{2.5}$ from the Guanzhong Plain: Chemical composition and implications for emission reductions, Atmos. Environ., 147, 458–469, https://doi.org/10.1016/j.atmosenv.2016.10.029, 2016.

Quan, J., Liu, Q., Li, X., Gao, Y., Jia, X., Sheng, J., and Liu, Y.: Effect of heterogeneous aqueous reactions on the secondary formation of inorganic aerosols during haze events, Atmos. Environ., 122, 306–312, https://doi.org/10.1016/j.atmosenv.2015.09.068, 2015.

Seinfeld, J. H. and Pandis, S. N.: Atmospheric chemistry and physics: From air pollution to climate change, third edn., John Wiley, New York, ISBN: 978-1-118-94740-1, 2006.

Shen, F., Zhang, L., Jiang, L., Tang, M., Gai, X., Chen, M., and Ge, X.: Temporal variations of six ambient criteria air pollutants from 2015 to 2018, their spatial distributions, health risks and relationships with socioeconomic factors during 2018 in China, Environ. Int., 137, 105556, https://doi.org/10.1016/j.envint.2020.105556, 2020.

Song, C., Wu, L., Xie, Y., He, J., Chen, X., Wang, T., Lin, Y., Jin, T., Wang, A., Liu, Y., Dai, Q., Liu, B., Wang, Y. N., and Mao, H.: Air pollution in China: Status and spatiotemporal variations, Environ. Pollut., 227, 334–347, https://doi.org/10.1016/j.envpol.2017.04.075, 2017.

Tan, J., Xiang, P., Zhou, X., Duan, J., Ma, Y., He, K., Cheng, Y., Yu, J., and Querol, X.: Chemical characterization of humic-like substances (HULIS) in PM$_{2.5}$ in Lanzhou, China, Sci. Total Environ., 573, 1481–1490, https://doi.org/10.1016/j.scitotenv.2016.08.025, 2016.

Tan, T., Hu, M., Li, M., Guo, Q., Wu, Y., Fang, X., Gu, F., Wang, Y., and Wu, Z.: New insight into PM$_{2.5}$ pollution patterns in Beijing based on one-year measurement of chemical compositions, Sci. Total Environ., 621, 734–743, https://doi.org/10.1016/j.scitotenv.2017.11.208, 2018.

Tang, K., Zhang, H., Feng, W., Liao, H., Hu, J., and Li, N.: Increasing but Variable Trend of Surface Ozone in the Yangtze River Delta Region of China, Frontiers in Environmental Science, 10, 836191, https://doi.org/10.3389/fenvs.2022.836191, 2022.

Tang, L., Qu, J., Mi, Z., Bo, X., Chang, X., Anadon, L. D., Wang, S., Xue, X., Li, S., Wang, X., and Zhao, X.: Substantial emission reductions from Chinese power plants after the introduction of ultra-low emissions standards, Nat. Energy, 4, 929–938, https://doi.org/10.1038/s41560-019-0468-1, 2019.

Tang, X., Chen, X., and Tian, Y.: Chemical composition and source apportionment of PM$_{2.5}$ – A case study from one year continuous sampling in the Chang-Zhu-Tan urban agglomeration, Atmos. Pollut. Res., 8, 885–899, https://doi.org/10.1016/j.apr.2017.02.004, 2017.

Tao, J., Zhang, L., Gao, J., Wang, H., Chai, F., and Wang, S.: Aerosol chemical composition and light scattering during a winter season in Beijing, Atmos. Environ., 110, 36–44, https://doi.org/10.1016/j.atmosenv.2015.03.037, 2015.

Tao, J., Zhang, L., Cao, J., Zhong, L., Chen, D., Yang, Y., Chen, D., Chen, L., Zhang, Z., Wu, Y., Xia, Y., Ye, S., and Zhang, R.: Source apportionment of PM$_{2.5}$ at urban and suburban areas of the Pearl River Delta region, south China – With emphasis on ship emissions, Sci. Total Environ., 574, 1559–1570, https://doi.org/10.1016/j.scitotenv.2016.08.175, 2017.

Tian, P., Wang, G., Zhang, R., Wu, Y., and Yan, P.: Impacts of aerosol chemical compositions on optical properties in urban Beijing, China, Particuology, 18, 155–164, https://doi.org/10.1016/j.partic.2014.03.014, 2015.

von Schneidemesser, E., Monks, P. S., Allan, J. D., Bruhwiler, L., Forster, P., Fowler, D., Lauer, A., Morgan, W. T., Paasonen, P., Righi, M., Sindelarova, K., and Sutton, M. A.: Chemistry and the Linkages between Air Quality and Climate Change, Chem. Rev., 115, 3856–3897, https://doi.org/10.1021/acs.chemrev.5b00089, 2015.

Wang, H., Tian, M., Chen, Y., Shi, G., Liu, Y., Yang, F., Zhang, L., Deng, L., Yu, J., Peng, C., and Cao, X.: Seasonal characteristics, formation mechanisms and source origins of PM$_{2.5}$ in two megacities in Sichuan Basin, China, Atmos. Chem. Phys., 18, 865–881, https://doi.org/10.5194/acp-18-865-2018, 2018.

Wang, H. L., Qiao, L. P., Lou, S. R., Zhou, M., Ding, A. J., Huang, H. Y., Chen, J. M., Wang, Q., Tao, S. K., Chen, C. H., Li, L., and Huang, C.: Chemical composition of PM$_{2.5}$ and meteorological impact among three years in urban Shanghai, China, J. Clean. Prod., 112, 1302–1311, https://doi.org/10.1016/j.jclepro.2015.04.099, 2016.

Wang, Y., Jia, C., Tao, J., Zhang, L., Liang, X., Ma, J., Gao, H., Huang, T., and Zhang, K.: Chemical characterization and source apportionment of PM$_{2.5}$ in a semi-arid and petrochemical-industrialized city, Northwest China, Sci. Total Environ., 573, 1031–1040, https://doi.org/10.1016/j.scitotenv.2016.08.179, 2016.

Wang, Y., Chen, J., Wang, Q., Qin, Q., Ye, J., Han, Y., Li, L., Zhen, W., Zhi, Q., Zhang, Y., and Cao, J.: Increased secondary aerosol contribution and possible processing on polluted winter days in China, Environ. Int., 127, 78–84, https://doi.org/10.1016/j.envint.2019.03.021, 2019.

Wu, J., Xu, C., Wang, Q., and Cheng, W.: Potential Sources and Formations of the PM$_{2.5}$ Pollution in Urban Hangzhou, Atmosphere, 7, 100, https://doi.org/10.3390/atmos7080100, 2016.

Wu, Y., Zhang, S., Hao, J., Liu, H., Wu, X., Hu, J., Walsh, M. P., Wallington, T. J., Zhang, K. M., and Stevanovic, S.: On-road vehicle emissions and their control in China: A review and outlook, Sci. Total Environ., 574, 332–349, https://doi.org/10.1016/j.scitotenv.2016.09.040, 2017.

Xu, H., Xiao, Z., Chen, K., Tang, M., Zheng, N., Li, P., Yang, N., Yang, W., and Deng, X.: Spatial and temporal distribution, chemical characteristics, and sources of ambient particulate matter in the Beijing-Tianjin-Hebei region, Sci. Total Environ., 658, 280–293, https://doi.org/10.1016/j.scitotenv.2018.12.164, 2019.

Yang, Y., Liao, H., and Lou, S.: Increase in winter haze over eastern China in recent decades: Roles of variations in meteorological parameters and anthropogenic emissions, J. Geophys. Res., 121, 13050–13065, https://doi.org/10.1002/2016jd025136, 2016.

Yang, S., Liu, Z., Li, J., Zhao, S., Xu, Z., Gao, W., Hu, B., and Wang, Y.: Insights into the chemistry of aerosol growth in Beijing: Implication of fine particle episode formation during wintertime, Chemosphere, 274, 129776, https://doi.org/10.1016/j.chemosphere.2021.129776, 2021.

Yu, S., Liu, W., Xu, Y., Yi, K., Zhou, M., Tao, S., and Liu, W.: Characteristics and oxidative potential of atmospheric PM2.5 in Beijing: Source apportionment and seasonal variation, Sci. Total Environ., 650, 277–287, https://doi.org/10.1016/j.scitotenv.2018.09.021, 2019.

Zhai, S., Jacob, D. J., Wang, X., Shen, L., Li, K., Zhang, Y., Gui, K., Zhao, T., and Liao, H.: Fine particulate matter (PM2.5) trends in China, 2013–2018: separating contributions from anthropogenic emissions and meteorology, Atmos. Chem. Phys., 19, 11031–11041, https://doi.org/10.5194/acp-19-11031-2019, 2019.

Zhang, H. and Li, H.: The source codes of the MTEA model, http://www.nuistairquality.com/m_tea, last access: 21 April 2022 (in Chinese).

Zhang, Q.: R & D and Application Demonstration of Dynamic Grid Emission Source Information Platform, The Fourth Technical Seminar on Emission Inventory of Air Pollution Sources in China, Nanjing, China, 18–19 September 2019 (in Chinese).

Zhang, Q., Streets, D. G., Carmichael, G. R., He, K. B., Huo, H., Kannari, A., Klimont, Z., Park, I. S., Reddy, S., Fu, J. S., Chen, D., Duan, L., Lei, Y., Wang, L. T., and Yao, Z. L.: Asian emissions in 2006 for the NASA INTEX-B mission, Atmos. Chem. Phys., 9, 5131–5153, https://doi.org/10.5194/acp-9-5131-2009, 2009.

Zhang, Q., Shen, Z., Cao, J., Zhang, R., Zhang, L., Huang, R. J., Zheng, C., Wang, L., Liu, S., Xu, H., Zheng, C., and Liu, P.: Variations in PM2.5, TSP, BC, and trace gases (NO2, SO2, and O3) between haze and non-haze episodes in winter over Xi'an, China, Atmos. Environ., 112, 64–71, https://doi.org/10.1016/j.atmosenv.2015.04.033, 2015.

Zhang, Y., Lang, J., Cheng, S., Li, S., Zhou, Y., Chen, D., Zhang, H., and Wang, H.: Chemical composition and sources of PM1 and PM2.5 in Beijing in autumn, Sci. Total Environ., 630, 72–82, https://doi.org/10.1016/j.scitotenv.2018.02.151, 2018.

Zhang, Y., Zhang, X., Zhong, J., Sun, J., Shen, X., Zhang, Z., Xu, W., Wang, Y., Liang, L., Liu, Y., Hu, X., He, M., Pang, Y., Zhao, H., Ren, S., and Shi, Z.: On the fossil and non-fossil fuel sources of carbonaceous aerosol with radiocarbon and AMS-PMF methods during winter hazy days in a rural area of North China plain, Environ. Res., 208, 112672, https://doi.org/10.1016/j.envres.2021.112672, 2022.

Zhang, Y. L. and Cao, F.: Fine particulate matter (PM2.5) in China at a city level, Sci. Rep., 5, 14884, https://doi.org/10.1038/srep14884, 2015.

Zhao, M., Huang, Z., Qiao, T., Zhang, Y., Xiu, G., and Yu, J.: Chemical characterization, the transport pathways and potential sources of PM2.5 in Shanghai: Seasonal variations, Atmos. Res., 158–159, 66–78, https://doi.org/10.1016/j.atmosres.2015.02.003, 2015.

Zhao, X. J., Zhao, P. S., Xu, J., Meng,, W., Pu, W. W., Dong, F., He, D., and Shi, Q. F.: Analysis of a winter regional haze event and its formation mechanism in the North China Plain, Atmos. Chem. Phys., 13, 5685–5696, https://doi.org/10.5194/acp-13-5685-2013, 2013.

Zhu, Y., Huang, L., Li, J., Ying, Q., Zhang, H., Liu, X., Liao, H., Li, N., Liu, Z., Mao, Y., Fang, H., and Hu, J.: Sources of particulate matter in China: Insights from source apportionment studies published in 1987–2017, Environ. Int., 115, 343–357, https://doi.org/10.1016/j.envint.2018.03.037, 2018.